Muscle-directed mechanosensory feedback activates egg-laying circuit activity and behavior in *C. elegans*

Emmanuel Medrano and Kevin M. Collins*

Department of Biology, University of Miami, Coral Gables, FL, United States of America

*Corresponding author. Email: kevin.collins@miami.edu

Abstract

Mechanosensory feedback of internal state regulates numerous bodily processes including feeding, defecation, and reproduction. However, how mechanosensory feedback signals to modulate neural circuits and coordinate these behaviors is incompletely understood. Here, we use the egg-laying circuit of *C. elegans* to test our hypothesis that mechanosensory feedback of egg accumulation promotes the active reproductive behavior state. Using an acute gonad microinjection technique to mimic changes in pressure and stretch resulting from germline activity and egg accumulation, we find that injection rapidly stimulates Ca^{2+} activity in both neurons and muscles of the egg-laying circuit. Injection-induced vulval muscle Ca^{2+} activity requires L-type Ca^{2+} channels but is independent of presynaptic input. Direct mechanical prodding activates the vulval muscles, suggesting they are the proximal targets of the stretch-dependent stimulus. Our results show that egg-laying behavior in *C. elegans* is regulated by a stretch-dependent homeostat that scales postsynaptic muscle responses with egg accumulation in the uterus.

INTRODUCTION

The ability to sense and convert physical stimuli into chemical signals that are then integrated and used to perform behavioral decisions is a conserved process that allows animals to survive and reproduce (Goodman and Sengupta, 2019). Mechanosensory feedback of internal reproductive state is crucial in shaping decisions about when to reproduce and where to rear offspring. For instance, the reduction in sexual receptivity of *Drosophila* following copulation is mediated by mechanosensory feedback (Shao et al., 2019). Following mating, the stretch produced from accumulated eggs in the reproductive tract is sufficient to induce an attraction to acetic acid to ensure oviposition occurs in favorable environments (Gou et al., 2014). Because artificial distention of the reproductive tract is sufficient to induce this attraction to acetic acid, feedback of egg accumulation itself drives the observed remodeling of sensory signaling. Likewise, mechanical stretch of the uterus is involved in initiating parturition or driving specific maternal behaviors like bonding or infanticide in various mammalian systems (Hayes and De Vries, 2007; Kendrick et al., 1991; Wray, 1993). Thus, while mechanical feedback of internal reproductive state exerts profound short- and long-term changes in neural circuit activity, the mechanosensory feedback mechanisms and circuits that mediate these processes are incompletely understood.

The *C. elegans* egg-laying circuit serves as an ideal system to study how different forms of mechanosensory feedback regulate reproductive behaviors. Previous work has shown that *C. elegans* egg laying is a stochastic, two-state behavior consisting of ~20 minute inactive states in which animals produce and retain eggs in the uterus punctuated by ~2 minute active states in which ~4-6 eggs are laid (Waggoner et

al., 1998). Egg laying is controlled by two motoneuron types, the serotonergic hermaphrodite-specific neurons (HSNs; Desai and Horvitz, 1989; Waggoner et al., 1998), and the cholinergic ventral type C (VC) neurons, both of which synapse onto the vulval muscles to promote contraction and egg laying (Bany et al., 2003; Collins et al., 2016; Shyn et al., 2003; White et al., 1986; Zhang et al., 2008). The cellular Ca^{2+} activity of several cells in the egg-laying circuit is regulated by mechanosensory feedback. For example, external vibrations or gentle touches on the tail inhibit egg laying (Sawin, 1996), possibly by activating mechanoreceptors on the PLM neurons that signal to inhibit HSN activity (Zhang et al., 2008). The VC neurons are mechanically activated by the contraction and opening of the vulval muscles, releasing acetylcholine to enhance vulval opening for egg release (Kopchock et al., 2021). The uv1 neuroendocrine cells sit between the vulval canal and uterus, are mechanically deformed and activated in response to passage of eggs through the vulval canal (Collins et al., 2016; Jose et al., 2007), and provide inhibitory feedback following egg laying through the release of tyramine and neuropeptides that inhibit HSN activity (Alkema et al., 2005; Banerjee et al., 2017; Ravi et al., 2021; Zhang et al., 2010). Whether other cells in the egg-laying circuit are mechanosensitive and how their feedback signals to modulate discrete steps in egg laying is not clear.

Our previous work demonstrated that feedback of egg accumulation regulates Ca^{2+} activity in the egg-laying circuit (Ravi et al., 2021, 2018a). Young adults or animals lacking eggs in the uterus have reduced Ca^{2+} activity in the HSNs, with the HSNs showing infrequent Ca^{2+} transients. Conversely, animals recovering from an acute blockage of egg laying show greatly increased Ca^{2+} transient activity and egg laying

68 (Ravi et al., 2018a). This homeostatic feedback to the HSNs depends on the
69 postsynaptic vulval muscles, as presynaptic HSN Ca^{2+} bursting activity is lost in Notch
70 receptor mutants (Li et al., 2013) lacking postsynaptic connection to the HSNs or when
71 the vulval muscles are electrically silenced (Ravi et al., 2018a). Together, these data
72 suggest that feedback of egg accumulation activates a stretch-dependent homeostat
73 that regulates circuit activity and serotonin release that sustains the egg-laying active
74 state. Interestingly, genetic ablation or electrical silencing of the HSNs delays, but does
75 not abolish, the onset of egg laying (Ravi et al., 2021, 2018a; Waggoner et al., 1998)
76 with animals recovering vulval muscle Ca^{2+} transient activity upon egg accumulation
77 (Collins et al., 2016). These results show that while feedback of egg accumulation can
78 promote HSN Ca^{2+} activity, HSN may not be its only target. However, the cellular and
79 molecular mechanisms underlying this putative stretch response remains unknown.
80 Here, we tested whether a stretch-dependent mechanism activates the *C.*
81 *elegans* egg-laying behavior circuit. Using acute microinjections to mimic feedback of
82 germline activity and embryo accumulation, we show that injection is sufficient to drive
83 both egg-laying circuit activity and behavior. Surprisingly, we find that animals deficient
84 in synaptic vesicle or peptidergic transmission still show an acute injection response.
85 This suggests that egg laying is at least partially driven by direct sensing of internal
86 stretch by the egg-laying vulval muscles. Furthermore, we show that the vulval muscles
87 themselves are receptive to direct mechanical stimulation and that L-type voltage-gated
88 calcium channels are required for Ca^{2+} influx. Together, our data reveal how
89 mechanosensory feedback, detected by the muscle target-cells, informs the circuit

90 whether there are eggs to lay that acts alongside synaptic input to induce egg-laying
91 behavior.

92 **RESULTS**

93 **Microinjections induce egg-laying behavior and circuit activity**

94 While microinjection into the gonad of *C. elegans* is a common technique for generating
95 transgenic strains (Berkowitz et al., 2008; Mello et al., 1991), we noticed this procedure
96 often led to vulval opening and egg release. While we feel this phenomenon is widely
97 known among *C. elegans* researchers, injection-induced egg laying is not well-
98 described in the literature. To determine that microinjection does stimulates egg laying,
99 we inserted a needle into the gonad syncytium of wild-type animals and performed a
100 brief (3 s) injection delivering ~250 pL of standard buffer lacking DNA while monitoring
101 egg release (**Figure 1A**). Microinjection drove egg laying in nearly half (~46 ± 9%) of
102 injected animals (**Figure 1B**). Egg-laying behavior in *C. elegans* is driven by Ca^{2+}
103 activity in the vulval muscles that drives contraction (Collins and Koelle, 2013; Shyn et
104 al., 2003; Zhang et al., 2008). To determine if egg release was a passive consequence
105 of injection or an active process driven by cellular activity, we performed ratiometric
106 Ca^{2+} recordings of the vulval muscles in animals expressing GCaMP5 (Collins et al.,
107 2016). Gonad injections triggered a strong and rapid induction of vulval muscle Ca^{2+}
108 activity which peaked on average 5.6 s after the onset of injection (**Figure 1C; Movie**
109 **1**). Direct contact with the injected buffer did not seem to be required for a robust
110 muscle response, as vulval muscle Ca^{2+} activity was induced immediately upon injection
111 while buffer reached the vulva a few seconds later (**Movie 1**). Egg-laying events were
112 coincident with peak vulval muscle Ca^{2+} activity (**Figure 1C**), similar to that seen

113 previously in behaving animals (Collins et al., 2016; Collins and Koelle, 2013). On
114 average, injection-induced vulval muscle Ca^{2+} transients decayed to 37% of their peak
115 value in 23 s. While the kinetic features of vulval muscle Ca^{2+} transient activity were
116 significantly longer than that seen in behaving animals (Collins et al., 2016), we
117 presume this is a consequence of the animals being immobilized during the injection
118 procedure as observed in previous studies (Shyn et al., 2003). Injections into *unc-*
119 *54(e190)* muscle-specific myosin mutants, in which the vulval muscles are unable to
120 contract, still triggered vulval muscle Ca^{2+} transients (**Figure 1 – figure supplement**
121 **1A**), but this activity was unable to drive egg release (**Figure 1B**), indicating that
122 microinjection does not simply force eggs out through the vulva. Together, these results
123 show that microinjection causes an active response, triggering a rapid onset of vulval
124 muscle Ca^{2+} activity whose magnitude can drive contractility and egg release.
125 To determine if the magnitude of stretch induced by injections affected the vulval
126 muscle Ca^{2+} response, we estimated the flowrates across multiple injections to
127 determine total volume delivered per injection. Injection flowrates ranged between ~10
128 and ~366 pL/s with a median of 82 pL/s, corresponding to a total volume delivered
129 ranging between 30 pL – 1 nL with a median of 246 pL for each 3 s injection (**Figure**
130 **1D**). We estimated the volume of one embryo to be ~25 pL, as such, our injections
131 corresponded to an equivalent stretch produced by the addition of 1.2 – 40 eggs (with a
132 median of ~10 egg-volumes per injection). To determine if this range of injection
133 volumes reflects a physiologically relevant number of eggs required to activate the
134 stretch-dependent homeostat, we determined the number of eggs accumulated in the
135 uterus at the onset of egg laying. Wild-type animals begin laying eggs at ~6 hours after

136 reaching adulthood, having accumulated ~8 eggs in the uterus (**Figure 1E**). We have
137 previously shown that the onset of egg laying is delayed in *egl-1(dm)* animals lacking
138 the HSN command neurons (Ravi et al., 2018a) and in animals with strongly reduced
139 HSN activity (Ravi et al., 2021). In HSN-deficient animals, the onset of egg laying is
140 delayed to ~20 hours after adulthood, a point when they have accumulated an average
141 of 45 eggs in their uterus (**Figure 1E**). We interpret this difference in ~37 eggs required
142 to activate egg laying in the absence of HSNs as providing a threshold estimate of how
143 much volume increase (~925 pL) is required to induce the stretch-dependent
144 homeostat. As such, the volumes typically injected in our experiments are quantitatively
145 similar to the volume changes that accompany egg production and induce egg laying *in*
146 *vivo*.

147 Do injections with greater volumes elicit a stronger vulval muscle Ca^{2+} response
148 and more frequent egg laying? To answer this question, we analyzed the correlation
149 between injection flowrate, injected at a range of 30 – 40 psi, and the resulting vulval
150 muscle Ca^{2+} peak amplitudes and probability of egg release. Linear and logistic
151 regressions showed no correlation between injection flowrate and vulval muscle Ca^{2+}
152 transient amplitude, nor between flowrate and egg release, respectively (**Figure 1 –**
153 **figure supplement 1B – C**). This lack of correlation indicates that the range of
154 flowrates in our 3 s injection protocol does not significantly affect the observed vulval
155 muscle Ca^{2+} transient responses. We observed that egg-laying events correlated with
156 larger vulval muscle Ca^{2+} peaks (**Figure 1F**), a result consistent with our previous
157 observations of *in vivo* Ca^{2+} imaging of the vulval muscles (Collins et al., 2016; Collins
158 and Koelle, 2013). Interestingly, the number of eggs accumulated in animals prior to

159 injection also correlated significantly with the resulting vulval muscle Ca^{2+} peak
160 amplitude elicited by injections (**Figure 1G**). This result suggests that animals with
161 greater egg accumulation at the time of injection were more likely to have stronger
162 vulval muscle Ca^{2+} transients, and therefore more likely to lay eggs, independent of
163 injection volume delivered (**Figure 1 – figure supplement 1C**). We explored additional
164 parameters that affected the injection response (**Figure 1 – figure supplement 1D – G;**
165 **see Methods**). Additional attempts to inject at low flowrates, with lower injection
166 pressures (25 psi instead of 30 – 40psi), while tracking liquid delivery with a fluorescent
167 reporter, revealed that the vulval muscle Ca^{2+} response was weaker when liquid
168 delivery was slow, independent of total volume delivered (**Figure 1 – figure**
169 **supplement 2E**). Injection pressures >30 psi used in all subsequent microinjection
170 experiments were above this threshold, allowing for rapid fluid delivery of >30 pL (~2
171 eggs) within 3 s and a reliable Ca^{2+} response (**Figure 1 – figure supplement 1B**).
172 Together, these results show that acute microinjection triggers rapid vulval muscle Ca^{2+}
173 activity that drives egg release. These results further suggest that microinjection may
174 activate the same homeostatic mechanism engaged by feedback of egg accumulation
175 in the uterus which promotes the egg-laying active state (Ravi et al., 2018a).

176

177 **The vulval muscle injection response is independent of egg availability and**
178 **neural circuit development**

179 As worms mature from juveniles to adults, the pattern of activity in the egg-laying circuit
180 also matures into clear active and inactive states. We have previously shown that
181 mature patterns of neural activity are dependent on the temporal development of the

182 worm as well as the presence of fertilized embryos (Ravi et al., 2018a). To test if the
183 vulval muscle Ca^{2+} response to acute injection was similarly dependent on egg
184 availability, we injected into adult worms lacking fertilized embryos or into L4 juvenile
185 worms that had not yet begun egg production. As shown in **Figure 2A**, we eliminated
186 fertilized egg accumulation either genetically using a sperm-deficient *fog-2* mutant
187 (Schedl and Kimble, 1988) or chemically with floxuridine (FUDR; Mitchell et al., 1979)
188 which disrupts proper formation of oocytes. We observed a strong induction of vulval
189 muscle Ca^{2+} activity following injections into either *fog-2* mutant or FUDR-sterilized
190 adults (**Figure 2B)**. While *fog-2* sperm-deficient mutant worms did not show any
191 significant differences compared to similarly injected wild-type control animals, Ca^{2+}
192 transient amplitudes in FUDR-sterilized animals were significantly increased (**Figure**
193 **2C**). Although these animals lacked embryos to lay, gonad injection still induced strong
194 contraction of the vulval muscles and vulval opening (data not shown). These results
195 show that adult animals lacking endogenous feedback of egg production and/or
196 accumulation in the uterus are still capable of mounting a robust vulval muscle Ca^{2+}
197 response to injection.
198 To determine if developmental age influenced vulval muscle activation, we
199 compared injection responses of juvenile animals at the late 4th larval (L4) stage to egg-
200 laying adults (picked 1 day earlier). Injections into late-L4 or adult animals showed
201 similar acute vulval muscle Ca^{2+} transient responses (**Figure 2D**) that were not
202 significantly different in amplitude (**Figure 2E**), although this Ca^{2+} activity in late-L4
203 juveniles was unable to drive vulval opening. Late-L4 juvenile animals showed a greater
204 variety of vulval muscle Ca^{2+} responses that led to a significant decrease in average

205 Ca^{2+} activity decay time (**Figure 2F**). We saw a similar heterogeneity in spontaneous
206 vulval muscle Ca^{2+} responses as they develop from L4 animals into adults, coincident
207 with induction of ERG K^+ channel expression in the vulval muscles (Ravi et al., 2018a).
208 Together, these results show that juvenile animals, prior to the onset of egg production,
209 or even sterile adults remain responsive to acute changes in internal pressure and/or
210 stretch that follow gonad microinjection.

211

212 **Microinjection induces sequential Ca^{2+} activity in other cells of the egg-laying**
213 **behavior circuit**

214 Egg laying in behaving animals is driven by a stereotypical pattern of rhythmic
215 and sequential cell Ca^{2+} activity. The HSN command neurons go first, with Ca^{2+}
216 transients peaking ~2 s before each egg-laying event when Ca^{2+} activity is seen to peak
217 in both the VC motor neurons and vulval muscles (Collins et al., 2016). uv1 Ca^{2+} activity
218 is last, typically peaking ~2 s after each egg-laying event (**Figure 3A**). To determine if
219 injection drives a similar, sequential pattern of Ca^{2+} activity, we performed injections in
220 animals expressing GCaMP reporters in either the HSNs, VCs, or uv1 cells. We found
221 that all cells of the circuit showed a robust induction of Ca^{2+} activity in response to
222 injection, but their order and kinetics of onset differed significantly from that seen in
223 behaving animals. The vulval muscles and uv1 neuroendocrine cells which sit proximal
224 to the vulval muscles showed the most rapid injection response (**Movie 2**), reaching
225 half-maximal Ca^{2+} levels at 2.4 ± 1.2 and 3.4 ± 3.3 s (mean ± SD), respectively, after the
226 onset of injection (**Figure 3B and 3C**). The VC neurons were next, showing a half-max
227 Ca^{2+} activity at 4.0 ± 1.5 s (**Figure 3D**; **Movie 3**). Surprisingly, the HSNs showed the

228 slowest response with half-max Ca^{2+} activity observed 6.4 ± 4.0 s (**Figure 3E and 3F**;
229 **Movie 4**). Injection-induced Ca^{2+} responses typically lasted longer and decayed more
230 slowly compared to those seen in freely behaving animals which may result from the
231 absence of rhythmic phasing of Ca^{2+} activity that accompanies locomotion (Collins et
232 al., 2016). The robust and rapid onset of vulval muscle Ca^{2+} activity upon acute
233 microinjection, and the out-of-sequence onset of activity seen in other cells in the circuit
234 (**Figure 3F**), suggests microinjection acts directly on the vulval muscles with Ca^{2+}
235 activity in the other cells of the circuit being a consequence of vulval opening and/or egg
236 laying.

237

238 **The vulval muscle microinjection Ca^{2+} response does not require synaptic or**
239 **peptidergic input**

240 To test the hypothesis that the vulval muscles respond to mechanical stretch cell-
241 autonomously, we removed synaptic and peptidergic input into the vulval muscles and
242 tested their Ca^{2+} response to microinjection. Specifically, we tested *egl-1(dm)* mutant
243 animals lacking HSNs and in which we blocked synaptic transmission from the VC
244 neurons through transgenic expression of Tetanus Toxin (**Figure 4A**). Despite lacking
245 most synaptic input and showing strong defects in egg laying, the vulval muscles of
246 these animals showed strong injection-induced Ca^{2+} activity and egg laying (**Figure**
247 **4B**). We observed no significant differences in the vulval muscle Ca^{2+} response time,
248 peak amplitude, decay time, or efficiency of injection-induced egg release when
249 compared to injected wild-type worms (**Figure 4C – F**). These results indicate the main
250 synaptic inputs into the vulval muscles are not required for the vulval muscle injection

251 response, consistent with previous work showing that worms lacking HSNs and/or VCs
252 still enter egg-laying active states (Waggoner et al., 1998) with robust vulval muscle
253 Ca^{2+} activity (Collins et al., 2016; Kopchock et al., 2021; Shyn et al., 2003; Zhang et al.,
254 2008).

255 To account for the possibility that other cells, including those outside the egg-
256 laying circuit, respond to acute injection and signal to activate the vulval muscles, we
257 injected into *unc-13(s69)* mutants lacking synaptic vesicle transmission (Richmond et
258 al., 1999) and *unc-31(e928)* mutants with defective dense core vesicle release (Ann et
259 al., 1997). Both mutants showed essentially normal vulval muscle Ca^{2+} responses after
260 acute microinjection (**Figure 4B – E**). In addition, these neurotransmission mutants
261 were just as likely to lay eggs in response to injection as wild-type animals (**Figure 4F**).
262 Together, these results show that the vulval muscles can respond to acute
263 microinjection independent of synaptic or peptidergic input. This suggests that the
264 injection-induced activation of egg-laying circuit activity is not simply a consequence of
265 nociceptive neuron activation but may instead represent a muscle-dependent
266 mechanism that detects acute changes in internal pressure or stretch that accompany
267 germline activity and egg accumulation.

268

269 **The vulval muscles are receptive to direct mechanical stimulation**

270 If the vulval muscles are direct targets of stretch being activated in response to acute
271 microinjection, they may respond to other forms of mechanical stimulation. We used a
272 glass capillary probe to prod either the anterior or posterior vulval muscles while
273 recording changes in muscle Ca^{2+} activity (**Figure 5A**). Mechanical stimulation of the

274 vulval muscles triggered a strong and immediate Ca^{2+} transient in the prodded vulval
275 muscles (**Figure 5B; Movie 5**). To determine optimal displacement distances, we
276 exposed animals to a train of prodding events in which each subsequent prodding event
277 displaced the vulval muscles by an additional 10 µm (ranging from 10 – 60 µm; **Figure**
278 **5C, top**). From this, we found that the vulval muscles responded most efficiently to 50
279 µm displacements (**Figure 5C, bottom**). We then applied 1 s, 50 µm prodding
280 stimulations and compared the induced Ca^{2+} responses in pairs of vulval muscles
281 where one set of muscles on either side of the vulval slit either did or did not receive the
282 prodding stimulus. We observed a significantly greater induction of Ca^{2+} in the vulval
283 muscles that were prodded (**Figure 5D – E**). Prodded muscles showed a half-maximal
284 Ca^{2+} response of 0.7 ± 0.4 s (mean ± SD). This response was faster than the observed
285 injection-induced response (2.4 ± 1.2 s), likely reflecting the difference in how the
286 mechanical stimulation is applied: direct (prodding) vs. indirect (injection). However,
287 unlike microinjections, direct vulval muscle prodding stimulations never led to egg-laying
288 events. This is consistent with previous work showing that successful egg-laying events
289 require coordinated contractions from both anterior and posterior vulval muscle groups
290 (Li et al., 2013). Together, these results demonstrate that the vulval muscles are
291 receptive to direct mechanical stimulation.

292

293 **L-type voltage-gated calcium channels are required for the vulval muscle**
294 **injection response**

295 Previous work has shown the mechanosensory neurons in *C. elegans* depend on Ca^{2+}
296 entry mediated by EGL-19, the sole L-type voltage-gated Ca^{2+} channel in *C. elegans*

297 (Frøkjær-Jensen et al., 2006; Suzuki et al., 2003). EGL-19 channels are expressed in
298 the vulval muscles and are required for proper egg laying (Kwok et al., 2006; Schafer et
299 al., 1996; Shyn et al., 2003; Trent et al., 1983). To test if the acute injection response
300 requires L-type voltage-gated Ca^{2+} channels, we recorded the vulval muscle Ca^{2+} in
301 animals where channel function was blocked genetically or pharmacologically (**Figure**
302 **6A**). Injection into *egl-19(n582)* loss-of-function mutants triggered vulval muscle Ca^{2+}
303 transients with significantly reduced amplitude (**Figure 6B – C**). Treatment of animals
304 with 25 μM nemadipine, a specific blocker of L-type Ca^{2+} channels (Kwok et al., 2006),
305 caused a dramatic and significant decrease in vulval muscle Ca^{2+} transient amplitude
306 following injection when compared to 0.1% DMSO controls (**Figure 6B – E; Movie 6**).
307 Injections were also less likely to elicit egg laying in nemadipine-exposed animals when
308 compared to DMSO-treated worms (**Figure 6F**). Interestingly, a small level of residual
309 Ca^{2+} activity that localized to the vm1 muscles was still observed in nemadipine-treated
310 animals (**Movie 6**). Whether this residual Ca^{2+} activity is caused by insufficient blocking
311 by nemadipine, differential expression of EGL-19 channels in the vm1 vs. vm2 vulval
312 muscles, or is mediated by other molecules, for example, Ca^{2+} influx mediated by
313 mechanoreceptors, is not yet clear. Nonetheless, these results indicate that L-type
314 voltage-gated Ca^{2+} channels are required for the normal injection-induced vulval muscle
315 response.

316

317 **TMC and PIEZO mechanosensitive channels are not required for the injection-**
318 **induced vulval muscle Ca^{2+} response**

319 PIEZO mechanosensitive ion channels have been previously shown to be expressed in

320 the reproductive system of *C. elegans*, including the vulva (Bai et al., 2020). To test if
321 Piezo channels mediate the injection-induced response we injected into *pezo-1(av149)*
322 mutants while recording vulval muscle Ca^{2+} activity. As shown in **Figure 7A**, injection
323 into *pezo-1* mutants led to robust vulval muscle Ca^{2+} responses with no significant
324 differences in peak amplitude (**Figure 7B**) or egg laying (**Figure 7C**) when compared to
325 wild-type animals. Thus, Piezo channels are not strictly required for the injection-
326 induced Ca^{2+} response seen in the vulval muscles.

327 Next, we sought to determine if TMC channels, a different class of ion channels
328 that contribute to mechanosensory responses (Pan et al., 2018), were mediating the
329 vulval muscle injection response. Within the egg-laying circuit of *C.* elegans, TMC-1 has
330 been previously shown to be expressed in both the HSNs and vulval muscles while
331 TMC-2 expression has only been found in the vulval muscles (Yue et al., 2018). Loss of
332 one or both channels leads to an egg-laying defective phenotype (Yue et al., 2018),
333 while *tmc-1* mutants have impaired inhibition of egg laying in response to harsh touch
334 (Kaulich et al., 2021), making these channels promising candidates for mediating a
335 stretch response. We injected into *tmc-1; tmc-2* double mutants while recording the
336 vulval muscle Ca^{2+} activity and egg-laying responses. Injections into *tmc-1*; *tmc-2*
337 mutants still led to a robust Ca^{2+} response (**Figure 7D**) which did not differ significantly
338 in peak amplitude (**Figure 7E**) or egg laying (**Figure 7F**) when compared to wild type
339 animals. Overall, these results indicate that neither Piezo nor TMC channels are
340 required for the vulval muscle injection-induced response.

341 **DISCUSSION**

342 We developed a quantitative microinjection technique to test whether acute
343 changes in mechanical stretch that might accompany egg accumulation drive the
344 activation of egg-laying behavior in *C. elegans*. We found that acute microinjection
345 induces Ca^{2+} activity in each cell of the egg-laying circuit along with efficient egg laying.
346 Surprisingly, we found that the vulval muscles, the final synaptic targets in the egg-
347 laying circuit, showed the strongest and most rapid Ca^{2+} responses. Injection-induced
348 vulval muscle Ca^{2+} activity did not require input from the HSNs or VC neurons and was
349 still observed in *unc-13* and *unc-31* mutant animals lacking synaptic or peptidergic
350 transmission, respectively. Direct prodding of the vulval muscles similarly induced Ca^{2+}
351 transient activity, suggesting the vulval muscles themselves are direct targets of a
352 stretch-homeostat that regulates egg laying. While the mechanosensory mechanism
353 that mediates the injection-induced response remains unclear, loss of TMC or PIEZO
354 channels did not significantly affect injection-induced vulval muscle Ca^{2+} responses.
355 However, we found vulval muscle Ca^{2+} transient responses were significantly
356 diminished by genetic or pharmacological inhibition of EGL-19 L-type voltage-gated
357 Ca^{2+} channels known to regulate egg laying *in vivo* (Schafer et al., 1996; Trent et al.,
358 1983). Together, these results support a model in which feedback of egg accumulation
359 in the uterus activates vulval muscle mechanoreceptors and L-type Ca^{2+} channels,
360 driving Ca^{2+} transient activity, contractility, and egg laying.

361 While there are numerous similarities between patterns of egg-laying circuit
362 activity seen in behaving animals and the acute injection response, the differences are
363 interesting and may help reveal the nature of the stretch-dependent homeostat.

364 Analysis of circuit Ca^{2+} activity in behaving animals shows frequent, rhythmic 'twitch'
365 Ca^{2+} transients in the vm1 vulval muscles phased with each body bend of locomotion
366 and stronger 'egg-laying' Ca^{2+} transients that contract both the vm1 and vm2 vulval
367 muscles (Brewer et al., 2019; Collins and Koelle, 2013). Injection-induced Ca^{2+}
368 transients are much longer (~20 s) than those seen in behaving animals (~2 s; Collins et
369 al., 2016). Similarly long Ca^{2+} transients have been previously reported in mechanically
370 activated neurons of immobilized animals (Suzuki et al., 2003) as well as from cells of
371 the egg-laying circuit (Shyn et al., 2003; Zhang et al., 2008). We propose that
372 locomotion provides additional negative feedback onto the egg-laying circuit, possibly to
373 reset activity in the circuit to allow subsequent bouts of egg release when the vulva can
374 open fully at a specific phase of the body bend (Collins and Koelle, 2013). In behaving
375 animals, Ca^{2+} activity in the HSN command neurons peaks about ~2 s before each egg-
376 laying event (Collins et al., 2016). In response to injection, we first observe Ca^{2+} activity
377 in the vulval muscles and the uv1s, followed by the VCs, and then finally in the HSNs.
378 We propose that serotonin and NLP-3 signaling from HSNs normally acts to increase
379 the electrical excitability of the vulval muscles already sensitized by stretch, as
380 optogenetic stimulation of the HSNs induces significantly weaker vulval muscle Ca^{2+}
381 responses in sterile animals (Ravi et al., 2018a). Injection bypasses HSNs, directly
382 activating a stretch signal on the vulval muscles that can drive contraction and egg
383 laying. Contraction of the vulval muscles then opens the vulva, activating tyramine and
384 neuropeptide release from the uv1 cells (Alkema et al., 2005; Banerjee et al., 2017;
385 Collins et al., 2016) which signal to inhibit HSN Ca^{2+} activity (Ravi et al., 2021). In this
386 model, rebound from fast-acting tyramine inhibition would allow subsequent egg-laying

387 events within each active state, while uv1-released neuropeptides drive long-term
388 inhibition to terminate the active state. Consistent with this idea, we see delayed onset
389 of HSN Ca^{2+} transient activity after injection, and vulval muscle Ca^{2+} transients in
390 subsequent injections are weaker in amplitude (**Figure 1 – supplementary Figure 1D**).

391 The robust injection response suggests the egg-laying circuit is primed to
392 respond to acute changes in embryo accumulation in the uterus. In support of this, *C.*
393 *elegans* typically lays 3 – 5 eggs about every 20-minutes (Waggoner et al., 1998) while
394 producing one egg from each gonad arm every 10 minutes (McCarter et al., 1999).
395 Thus, the egg-laying rate is matched by the rate of egg production and, as such,
396 dramatic swings in egg accumulation are normally small and likely averaged out over
397 the 12-15 eggs found in the uterus at steady-state. Deposition of one or more eggs into
398 the uterus from the spermatheca (McCarter et al., 1999), or detection of some critical
399 stretch threshold by unidentified cells, may serve as an acute stretch signal to induce
400 the active state. This is supported by our analyses of the effects of flowrate on Ca^{2+}
401 transient amplitude and egg-laying responses. We find a wide range of flowrates are
402 equally as likely to induce a strong vulval muscle Ca^{2+} transient sufficient to drive egg
403 release (**Figure 1 – figure supplement 1B**), indicating that stretch induced by our
404 injections is above a critical threshold. Future studies will focus on establishing a stretch
405 threshold for egg-laying behavior while identifying the molecular basis for this threshold.

406 The ability of the vulval muscles to respond to the injection stimulus independent
407 of synaptic input suggests a bottom-up control of egg laying wherein stretch caused by
408 egg accumulation activates the vulval muscles and egg laying. This mechanism of
409 control is commonly found in various autonomic functions such as the myogenic reflex

410 that detects stretch in the gut (Alvarez, 1922; Mercado-Perez and Beyder, 2022),
411 baroreceptor reflex that maintains arterial pressure (Guyton, 1976; Kandel et al., 2012),
412 and micturition reflex that detects bladder stretch (Guyton, 1976). Decoupling of
413 feedback from these cells to higher control centers does not abolish the reflex but
414 removes the ability of higher control centers to regulate and maintain homeostasis. For
415 example in micturition, damage to the spinal cord above the sacral region leads to loss
416 of faciliatory inputs from the brain and causes an initial suppression of the micturition
417 reflex that is eventually restored over time (Guyton, 1976). A strikingly similar pattern
418 occurs in the egg-laying circuit of *C. elegans* as removal of the HSN command neurons
419 leads to a marked reduction in the frequency of egg-laying active states (Waggoner et
420 al., 1998) and a dramatic delay in the onset of egg laying (Ravi et al., 2018a) which is
421 restored only after the accumulation of 45 eggs (**Figure 1E**) when vulval muscle Ca^{2+}
422 activity resumes active / inactive state behavior transitions. Similarly, injection can
423 bypass the absence of synaptic input from the HSN command neurons, although we
424 expect that sensory feedback onto the HSNs ensures that eggs are normally laid in
425 favorable environmental conditions (Fenk and de Bono, 2015; Hallem and Sternberg,
426 2008; Ringstad and Horvitz, 2008). Thus, it is likely that feedback from a similar bottom-
427 up mechanism informs the HSNs of egg availability to ensure a transition into and out of
428 egg-laying active states.

429 What is the molecular mechanism mediating the injection-induced vulval muscle
430 response? While L-type calcium channels mediate mechanosensory responses in
431 mechanosensitive neurons of *C. elegans*, these channels have not previously been
432 shown to be mechanosensitive in *C. elegans*. However, in the human GI tract, $Ca_v1.2$ L-

433 type voltage-gate Ca^{2+} channels have been shown to be activated by increases in
434 intracellular pressure and by mechanical shear stress (Alcaino et al., 2017; Farrugia et
435 al., 1999). Mechanosensitivity was retained by the α_{1c} subunit of $Ca_v1.2$ during
436 heterologous expression in HEK-293 or CHO cells (Lyford et al., 2002). L-type calcium
437 channels have also been shown to be required for the mechanosensitive response of
438 rat cardiomyocytes (Takahashi et al., 2019). Given the expression of EGL-19 L-type
439 Ca^{2+} channels in the vulval muscles and other cells of the egg-laying circuit (Taylor et
440 al., 2021), stretch produced by accumulation of eggs may directly modulate the opening
441 of L-type Ca^{2+} channels to excite the vulval muscles. However, this work cannot rule out
442 previously proposed models in which serotonin-mediated activation of EGL-19
443 channels, through a $G\alpha_q$-signaling pathway, indirectly promotes egg laying via an
444 increase in the excitability of the vulval muscles (Dhakal et al., 2022; Schafer, 2006;
445 Waggoner et al., 1998). This model would predict that lack of an injection-induced
446 response after L-type Ca^{2+} channel block is a consequence of reduced vulval muscle
447 excitability. As such, future work should focus on determining the role of EGL-19 L-type
448 voltage-gated calcium channels in regulating vulval muscle excitability and their
449 potential mechanosensitive role in *C. elegans*.

450 Gap junctions may also be important molecules driving the vulval muscle
451 injection-induced Ca^{2+} response. The vulval muscles show extensive electrical coupling
452 via gap junctions among themselves and with other cells (Cook et al., 2019; White et al.,
453 1986), with the vm2 vulval muscles making gap junctions both with the uterine muscles
454 and the vm1 muscles where we observe rhythmic input during locomotion (Collins et al.,
455 2016). In this model, egg accumulation activates mechanoreceptors on the uterine

456 muscles, leading to the spread of electrical excitation through gap junctions into the vm2
457 vulval muscle 'hub' to induce the active state, as seen previously for the extensively
458 gap-junctioned RMG neurons that facilitate pheromone attraction (Macosko et al.,
459 2009). Once eggs are laid and the stretch signal is lost, excitation is shunted out of the
460 vulval muscles, making it harder for the circuit to remain in the active state, similar to the
461 electrical shunting mechanism that mediates touch perception in the nose touch hub-
462 and-spoke circuit of *C. elegans* (Rabinowitch et al., 2013). Egg-induced stretch signals
463 may also feedback onto the egg-laying neurons as the HSN and VC neurons express
464 several innexins (Altun et al., 2009; Taylor et al., 2021) and make gap junctions among
465 themselves, between each other, and with VC3 making a gap junction with the vm2
466 muscles (White et al., 1986). Interestingly, UNC-7 innexins have been recently shown to
467 function as mechanosensitive hemichannels (Walker and Schafer, 2020), suggesting a
468 possible mechanosensory role for other innexins expressed in the egg-laying circuit.

469 *C. elegans* egg-laying behavior is regulated by a variety of external sensory cues
470 including environmental CO_2 (Fenk and de Bono, 2015; Hallem and Sternberg, 2008),
471 male pheromones (Aprison and Ruvinsky, 2019), mechanical stimulation (Sawin, 1996),
472 food availability (Trent, 1982), and osmolarity (Zhang et al., 2008). The regulation of egg
473 laying via changes in osmotic conditions is particularly interesting in the context of our
474 results. While the molecular and cellular mechanisms by which osmolarity regulates egg
475 laying are unclear, it is interesting that osmotic regulation of egg laying might have the
476 same physical consequences as acute injection. Shifting *C. elegans* into hypoosmotic or
477 hyperosmotic environments results in inhibition or promotion of egg laying, respectively
478 (Zhang et al., 2010, 2008). Given that *C. elegans* is hydrostatically pressurized (Avery

479 and Thomas, 1997; Gilpin et al., 2015; Harris and Crofton, 1957), and vulval opening is
480 sufficient for egg expulsion from the uterus (Kopchock et al., 2021), changes in osmotic
481 conditions may reflect a physical regulation of egg-laying behavior. Acute shifts of
482 animals to hypoosmotic conditions drives a rapid influx of water into animals (Lamitina
483 et al., 2004) that presumably increases the hydrostatic pressure inside the animal, thus
484 promoting circuit activity and egg-laying based on a physical model. Conversely, a
485 decrease in hydrostatic pressure would similarly be predicted to inhibit egg-laying circuit
486 activity and behavior, as previously observed (Zhang et al., 2010, 2008). Our data
487 shows that the initial level of egg accumulation is a primary predictor for vulval muscle
488 Ca^{2+} transient amplitude and the probability for an egg-laying response. Future work
489 should test whether the hydrostatic pressure gradient is used to drive physical expulsion
490 of eggs in response to vulval opening.

491 Overall, our work reveals a new model by which egg laying is regulated in *C.*
492 *elegans*. Sensory feedback converges at the HSN command neurons, regulating
493 serotonin and neuropeptide release, informing the circuit about favorable environmental
494 conditions, e.g., the external state. This top-down processing decides ‘when’ and
495 ‘where’ egg laying should occur. Feedback of germline activity and egg accumulation
496 directly stimulates the vulval muscles, communicating information to the circuit about
497 the internal state, namely that the animal has eggs to lay. This ‘bottom-up’ processing
498 determines ‘if’ and ‘for how long’ eggs can be laid. These distinct forms and sources of
499 modulatory input help drive optimal patterns of circuit activity that allow animals to
500 adjust their behavior to a changing environment.

501 **Materials and Methods**

502 **Nematode culture and staging**

503 *Caenorhabditis elegans* strains were grown at 20°C on Nematode Growth Medium
504 (NGM) agar plates with *E. coli* OP50 grown in B broth as a food source (Brenner, 1974).
505 All assays involving adult animals were performed using adult hermaphrodites staged
506 24 h past the late L4 larval stage. For assays involving L4 animals, late-stage L4 worms
507 were picked 30 minutes prior to the assay. A list of strains, mutants, and transgenes
508 used in this study can be found in **Table 1**.

509 **Calcium reporter transgenes and strain construction**

510 Vulval muscle Ca^{2+}

511 Vulval muscle Ca^{2+} activity was recorded in adult animals using LX1918 *vsIs164 [unc-*
512 *103e::GCaMP5::unc-54 3'UTR + unc-103e::mCherry::unc-54 3'UTR + lin-15(+)]*, *lite-*
513 *1(ce314), lin-15(n765ts) X*, as described (Collins et al., 2016). Because the *unc-103e*
514 promoter does not express strongly in the vulval muscles of younger L4 animals (Ravi
515 et al., 2018a), MIA51 *keyIs12 [ceh-24::GCaMP5::unc-54 3'UTR ceh-24::mCherry::unc-*
516 *54 3'UTR lin-15(+)] IV, lite-1(ce314), lin-15(n765ts) X*, as described (Ravi et al., 2018a)
517 was used in experiments comparing injection responses in late L4 animals.

518 To image vulval muscle Ca^{2+} activity in animals defective for muscular
519 contractions, MIA206 [*unc-54(e190) I; vsIs164 X lite-1(ce314) lin-15(n765ts) X*] strain
520 was generated. To generate this strain, LX1918 males were crossed with CB190 [*unc-*
521 *54(e190) I*] myosin heavy chain null mutant hermaphrodites (Brenner, 1974; Dibb et al.,
522 1985). Offspring were allowed to self and uncoordinated, mCherry(+) F2 progeny were
523 then selected and allowed to self for multiple generations until both phenotypes were

524 observed to be homozygous.

525 To record Ca^{2+} activity from the vulval muscles of animals lacking fertilized
526 embryos, BS553 [*fog-2(oz40) V)*] spermatogenesis mutant (Schedl and Kimble, 1988)
527 males were crossed with LX1918 hermaphrodites. Cross-progeny hermaphrodites were
528 picked and were crossed back to BS553 *fog-2* males to generate mCherry(+), *fog-2/+*
529 males and mCherry(+), *fog-2* hermaphrodites which were identified from single
530 mCherry(+) L4 hermaphrodites that then developed into sterile, *fog-2* adults. Male and
531 hermaphrodite progeny continued to be crossed until the *fog-2*, mCherry(+) phenotypes
532 were homozygous. The resulting strain, MIA34 [*fog-2(oz40) V; lite-1(ce314) lin-15(n765)*
533 *vsIs164 X*], was then maintained by male and female self-progeny.

534 To determine if injection-induced vulval muscle Ca^{2+} responses were dependent
535 on input from the HSNs or VC neurons, a strain lacking HSNs while simultaneously
536 expressing Tetanus Toxin in the VC neurons was generated. To do this, N2 males were
537 crossed with the HSN-deficient LX1938 *egl-1(n986dm) V; lite-1(ce314) vsIs164 lin-*
538 *15(n765ts) X* hermaphrodites (Collins et al., 2016). Resulting male cross-progeny were
539 then mated with MIA144 *keyIs33; lite-1(ce314) lin15(n765ts) X* hermaphrodites
540 (Kopchock et al., 2021) expressing Tetanus Toxin in the VC neurons from a minimal *lin-*
541 *11* enhancer (Bany et al., 2003) which imparts a mild uncoordinated reversal
542 phenotype. Resulting cross-progeny L4s were then picked, allowed to self, and were
543 then selected for mCherry(+), Egl, and Unc reversal phenotypes. Animals were then
544 positively genotyped for *egl-1(n986dm)* using the following oligos: 5'-CTC TGT TCC
545 AGC TCA AAT TTC C-3' (forward) and 5'-GTA GTT GAG GAT CTC GCT TCG GC-3'
546 (reverse) followed by NciI enzyme digestion. Confirmed homozygous animals were kept

547 as strain MIA289 *keyIs33; egl-1(n986dm) V; vsIs164 lite-1(ce314) lin-15(n765ts) X*.

548 To eliminate neuropeptide signaling while monitoring injection-induced Ca^{2+}

549 activity in the vulval muscles, the dense core vesicle release mutant, CB928 *unc-*

550 *31(e928) IV* (Brenner, 1974), was crossed with LX1918 males. *vsIs164* mCherry(+)

551 hermaphrodite cross-progeny were allowed to self and were then selected for

552 mCherry(+), Unc*,* and Egl phenotypes, resulting in strain MIA312 [*unc-31(e928) IV;*

553 *vsIs164 X; lite-1(ce314) lin-15(n765ts) X*]. Similarly, to eliminate neurotransmitter

554 release while monitoring injection-induced Ca^{2+} activity from the vulval muscles, the

555 neurotransmitter release mutant, EG9631 [*unc-13(s69) I*] (Rose and Baillie, 1980), was

556 crossed with *vsIs164* mCherry(+) males. mCherry(+) hermaphrodite cross-progeny

557 were picked as L4s, allowed to self, and mCherry(+), Unc F2 progeny were kept,

558 resulting in strain MIA316 *unc-13(s69) I; vsIs164 lite-1(ce314) lin-15(n765ts) X*.

559 To image Ca^{2+} activity in the vulval muscles of animals lacking the EGL-19, L-

560 type voltage-gated Ca^{2+} channel (Trent et al., 1983), LX1918 males were crossed with

561 MT1212 *egl-19(n582) IV* hermaphrodites. Cross-progeny were isolated and allowed to

562 self and resulting mCherry(+) non-Egl progeny were picked and allowed to self until

563 homozygous for mCherry(+) and Egl phenotypes. The resulting strain MIA185 (*egl-*

564 *19(n582) IV; lite-1(ce314) lin-15(n765ts) vsIs164 X*) was used in this study.

565 To monitor Ca^{2+} activity in the vulval muscles of mechanosensory mutants,

566 *vsIs164* males were crossed with *pezo-1* mutants provided by Drs. Xiaofei Bai and Andy

567 Golden (Bai et al., 2020). This resulted in the generation of the AG527 strain [*pezo-1*

568 *(av149) IV; vsIs164 lite-1(ce314) lin-15(n765ts) X.*

569 To visualize vulval muscle Ca^{2+} activity in *tmc-1*, *tmc-2* mechanosensory

570 mutants, N2 males were crossed with LX1919 *vsIs165 [unc-103e::GCaMP5::unc-54*
571 *3'UTR + unc-103e::mCherry::unc-54 3'UTR + lin-15(+) ; lite-1(ce314) lin-15(n765ts) X]*
572 hermaphrodites (Collins et al., 2016; Ravi et al., 2021). mCherry(+) *vsIs165/+* male
573 cross-progeny were then crossed with RB1546 *tmc-1(ok1859) X* hermaphrodites.
574 mCherry(+) cross-progeny hermaphrodites were then picked and allowed to self.
575 mCherry(+) cross-progeny were then genotyped for *tmc-1(ok1859)* using a duplex PCR
576 strategy with the following primers: 5'-CGA CTA CTG CAA TTC TCT TTA AGG-3'
577 (outside forward), 5'-GTT TAC AGT ATA CAA AAT TAG GAC TCT G-3' (inside
578 reverse), 5'-GTG CAG TAC ATT CTC CGC CAC C-3' (outside reverse), generating
579 MIA486 *vsIs165*; *tmc-1(ok1859) X* strain used in this study. To generate MIA487
580 *vsIs165 tmc-2(ok1302) X*, the same approach was used but the RB1237 *tmc-2(ok1302)*
581 *X* hermaphrodites was used instead when crossed with *vsIs165/+* males. mCherry(+)
582 progeny were confirmed to be homozygous for *tmc-2(ok1302)* using the following
583 primers: 5'-CAA TCG TCG TGG GAC CTT ATC ATC-3' (outside forward), 5'-CTA CAG
584 TGT CAT TAC TGA TGT TCT TC-3' (inside forward), 5'-CTC TTC TGT CCG TTC CTG
585 GAA ATG-3' (outside reverse). During construction of MIA486 and MIA487, we noticed
586 the loss of the *lite-1(ce314) X* mutation present in the original LX1919 starting strain as
587 *tmc-1* and *tmc-2* genes, both of which are near *lite-1*, were being homozygosed. To
588 account for any changes in vulval muscle Ca^{2+} activity that arise from blue light
589 illumination rather than acute injection, a control strain MIA485 *vsIs165* was generated
590 by crossing N2 males with LX1919 hermaphrodites. Heterozygous cross-progeny
591 hermaphrodites with mCherry expression were selected, selfed, and loss of *lite-*
592 *1(ce314)* in the progeny was confirmed through genotyping.

593 MIA494 *vsIs165*; *tmc-1(ok1859) tmc-2(ok1302) X* was generated to image vulval
594 muscle Ca^{2+} activity in animals lacking both TMC-1 and TMC-2. Briefly, N2 males were
595 mated to RB1546 *tmc-1(ok1959)* hermaphrodites, and the resulting hemizygous (*tmc-*
596 *1/Ø*) males were then crossed with MIA487 hermaphrodites. The resulting cross-
597 progeny were then allowed to self until *tmc-1* and *tmc-2* mutations were confirmed to be
598 homozygous through genotyping.

599 <u>uv1 neuroendocrine cell Ca^{2+}</u>

600 Ca^{2+} activity of uv1 neuroendocrine cells was monitored in adult animals using MIA136
601 *keyIs34 lite-1(ce314) lin-15(n765ts) X* which expresses GCaMP5 and mCherry from the
602 *tdc-1* promoter (Alkema et al., 2005) which provides stronger uv1 expression compared
603 to the *ocr-2* promoter previously used (Collins et al., 2016). To generate this strain, the
604 *ocr-2* promoter was replaced with a 1.5 Kb region of the *tdc-1* promoter amplified from
605 *Ptdc-1::ChR2* generously provided by Mark Alkema using oligonucleotides Ptdc-1new-
606 fwd: GCG GCA TGC CAC CTA ACT TCG TCG GTC and Ptdc-1-new-rev: GCG CCC
607 GGG GAT CCT TGG GCG GTC CTG, digested with SphI/XmaI, and ligated into
608 similarly digested pKMC281 [*Pocr-2::mCherry::ocr-2(3'UTR)*] or pKMC284 [*Pocr-*
609 *2::GCaMP5::ocr-2(3'UTR)*], generating pAB5 [*Ptdc-1::mCherry::ocr-2(3'UTR)*] and pAB6
610 [*Ptdc-1::GCaMP5::ocr-2(3'UTR)*]. pAB5 [*Ptdc-1::mCherry* (5 ng/μL)], pAB6 [*Ptdc-*
611 *1::GCaMP5* (20 ng/μL)], and pL15EK (50 ng/μL) were injected into LX1832 *lite-*
612 *1(ce314), lin-15(n765ts)* animals, generating the extrachromosomal transgene *keyEx28*
613 which demonstrated bright and specific expression in the uv1 cells along with dim
614 expression in the RIM neurons. This transgene was then integrated to chromosomes

615 using UV/TMP to generate four independent integrants *keyIs34–37*, of which *keyIs34*
616 was used for this study.

617 VC Ca^{2+}

618 Ca^{2+}activity in the VC neurons was monitored in adult animals using strain LX1960
619 *vsIs172; lite-1(ce314) lin-15(n765ts) X,* as described (Collins et al., 2016). Ca^{2+} activity
620 levels were averaged from all VC cell bodies and process (VC1-VC6). However, due to
621 expression patterns, differences in focus, and the position of worms during recording,
622 not all VCs were captured in all experiments, especially VC1 and VC6 which are more
623 distant from the vulval-proximal VC4 and VC5.

624 HSN Ca^{2+}

625 Ca^{2+} activity in the HSNs was monitored in adult animals using LX2004 *vsIs183 lite-*
626 *1(ce314) lin-15(n765ts) X,* as described (Collins et al., 2016; Ravi et al., 2018b).

627 **Egg accumulation at onset of egg laying**

628 To determine the extent of egg accumulation at onset of egg laying, both wild-type and
629 MIA26 *egl-1(n986dm)* mutant animals were staged following the L4 molt as previously
630 described (Ravi et al., 2018a). Animals were observed for the first instance of egg laying
631 every 30 minutes (after a 4 h period for wild type and after a 16 h period for *egl-1(dm)*
632 mutants). Once an animal had laid its first egg, it was dissolved in a 20% bleach
633 solution, and the eggs in the uterus were counted as described (Chase and Koelle,
634 2004). The number of eggs in the uterus plus the number of eggs laid on the plate were
635 considered the total number of eggs accumulated at the onset of egg laying.

636

637 **Microinjection protocol and flowrate estimate**

638 To induce acute increases in pressure within *C. elegans* worms, we performed
639 microinjections essentially as described (Berkowitz et al., 2008). To create
640 microinjection needles, filamented glass capillaries (4”, 1.0 mm outer diameter; World
641 Precision Instruments, 1B100F-4) were pulled using a Sutter P-97 Flaming/Brown type
642 micropipette puller using a custom program with the following parameters: Pressure =
643 500, Heat = 632 (ramp test value), Pull = 45, Velocity = 75, Delay = 90. Needles were
644 back-filled with injection buffer (2% polyethylene glycol, 20 mM potassium phosphate, 3
645 mM potassium citrate, pH 7.5) and then placed into a Narishige HI-7 injection holder.
646 Worms were injected using a Narishige IM-300 pneumatic microinjector with injection
647 pressure between 30 – 40 psi, unless otherwise noted. Injections were programmed for
648 a 3 s injection pulse and initiated manually using a foot pedal. To synchronize injection
649 onset with captured brightfield and fluorescence micrographs, the ‘sync’ voltage signals
650 of the microinjector were controlled and/or monitored using an Arduino Uno
651 microcontroller running the Firmata library in Bonsai (Lopes et al., 2015). Injections (3 s)
652 were triggered either using a foot-pedal or a TTL digital pin, and the timing of injection
653 onset was recorded using an analog pin. To assess consistency of injection needles,
654 the average flowrate of needles was calculated from brightfield recordings by measuring
655 the volume of a spherical drop of injection buffer injected into halocarbon oil. The
656 volume was calculated by measuring the expanding diameter of the drop in the first 20
657 frames of a three second injection (10 msec exposures recorded at 20 Hz). The

658 average flowrate of multiple needles pulled using this protocol was calculated to be 47
659 pL/s with a standard deviation of 15 pL/s (n = 10).

660 To perform microinjections, worms were placed into a small drop of halocarbon oil on a
661 2% agarose pad to immobilize them (Berkowitz et al., 2008). Animals were then placed
662 onto an inverted Zeiss Axio Observer.Z1 fluorescence microscope for imaging. A
663 Narishige coarse manipulator (model MMN-1) and a Narishige three-axis oil hydraulic
664 micromanipulator (model MMO-203) were used to position the tip of the needle next to
665 the gonad of the worm. Needles were then introduced along the dorsal surface into
666 either anterior or posterior gonad of the worm before initiating the recording (see
667 fluorescence imaging). The first 3 s injection was triggered 30 seconds after the onset of
668 synchronous brightfield and fluorescence recording. Subsequent injections were
669 performed in one-minute intervals. Before the end of the recording, the injection needle
670 was withdrawn from each animal, and the flowrate of the needle was once again
671 recorded to determine if the flowrate had changed materially during the injection. The
672 median flowrate from a subsample of 104 animal injections was 82 pL/s and ranged
673 between 10 and 365 pL/s. Such variation was seen to result from either needle tips
674 clogging or being open further as a consequence of injection, but this variability did not
675 seem to alter injection-induced responses (see optimization of microinjection protocol).

676 **Brightfield and fluorescence recordings**

677 To record egg-laying behavior during injections, a Grasshopper 3 camera (FLIR) was
678 used to capture 2 x 2 binned, 1,024 x 1,024 8-bit JPEG image sequences. Vulval
679 muscle, HSN, VC, or uv1 Ca^{2+} responses were recorded as described (Collins et al.,
680 2016; Ravi et al., 2018b). GCaMP5 and mCherry fluorescence was excited at 470 nm

681 and 590 nm, respectively, for 10 msec using a Colibri.2 LED illumination system.
682 Recordings were collected at 20 fps and a 256x256 pixel resolution (4x4 binning) using
683 a Hamamatsu Flash 4.0 V2 sCMOS camera recording at 16-bit depth through a 20x
684 Apochromatic objective (0.8NA). GCaMP5 and mCherry channels were separated via a
685 Gemini beam-splitter. Worms were recorded for 30 seconds prior to injection to
686 establish baseline levels of cell activity and were completed within five minutes to
687 reduce effects from worm desiccation after prolonged exposure to halocarbon oil. Image
688 sequences were imported into Volocity (Version 6.5.1, Quorum Technologies Inc.) for
689 GCaMP5/mCherry ratiometric analysis, image segmentation, Ca^{2+} quantitation of
690 GCaMP5/mCherry ratio changes ($\Delta R/R$), and Ca^{2+} transient peak finding, as described
691 previously (Collins et al., 2016; Ravi et al., 2018b).

692 **Optimization of microinjection protocol**

693 To ensure injections into control animals and the different mutants were comparable,
694 the correlation between flowrate and recorded calcium transient amplitudes was
695 analyzed. From this comparison, we found that flowrate had no significant effect on the
696 amplitude of the resulting vulval muscle Ca^{2+} transients **(**p-value = 0.5816; **Figure 1 –**
697 **figure supplement 1B)** and, as a result, the injection flowrate was allowed to vary.
698 Additionally, the correlation between flowrate and an egg-laying response was also
699 analyzed. This relationship also showed no significant correlation after performing a
700 logistic regression on the data (p-value = 0.0712; **Figure 1 – figure supplement 1C**).
701 Individual animals were injected multiple times to determine if subsequent responses
702 were comparable. We found that subsequent injections resulted in lower Ca^{2+} transient
703 amplitudes and were also less likely to result in an egg-laying event **(Figure 1 – figure**

704 **supplement 1D)**. However, given the wide range of flowrates obtained among multiple
705 injections, we limited our analyses of injection-induced Ca^{2+} responses to each animal's
706 first injection.

707 To determine if the composition of the injection buffer influenced the Ca^{2+}
708 response, worms were injected with deionized water or Milli-Q water. Injections with
709 both types of water did not differ in their ability to induce comparable levels of Ca^{2+}
710 transient activity from the vulval muscles (p-value >0.05; **Figure 1 – figure supplement**
711 **1E**). However, we observed that when the injection buffer was made with Na^+ salts
712 instead of K^+ salts, a decrease in the average vulval muscle Ca^{2+} response was
713 observed (p-value = 0.0003; **Figure 1 – figure supplement 1E**) when compared to the
714 standard K^+ salt containing buffer. To ensure that the injection-induced response is not
715 a consequence of a disruption of the Na^+/K^+ gradient, low flowrate injections were
716 performed by decreasing injection pressure to 20 psi. In these low-flow experiments, we
717 observed that injections were more likely to fail to elicit a Ca^{2+} response even when the
718 'optimal' K^+ buffer was used. Injections were performed into either the anterior or
719 posterior gonad, with no significant difference in vulval muscle Ca^{2+} transient amplitude
720 or proportion of injection-induced egg laying observed (**Figure 1 – figure supplement**
721 **1F – G**). Attempts to determine if injections performed in other compartments (e.g. the
722 uterus) also drove vulval muscle Ca^{2+} activity were unsuccessful due to injection
723 needles frequently getting clogged (data not shown).

724 <u>Injections with bromophenol blue</u>

725 To visualize injections, and to determine if Ca^{2+} dynamics correlated with the rate of
726 liquid spread at lower flowrates (injection pressure 25 psi), a solution of 450 μM

727 bromophenol blue made in injection buffer was used as a fluorescent tracker (**Figure 1**
728 **– figure supplement 2A**). Bromophenol blue was excited at 590 nm alongside co-
729 expressed mCherry and collected through the same mCherry filter set. To determine if
730 the flowrate of injections influenced vulval muscle Ca^{2+} responses, worms were
731 manually injected (25 psi) by depression of the foot pedal until the bromophenol
732 fluorescence was seen by eye to reach the vulval muscles (**Figure 1 – figure**
733 **supplement 2A**). Bromophenol fluorescence was then quantified in Volocity. The Sum
734 of individual pixel intensities was used as a proxy of total volume delivered during the
735 course of each injection [(pixel area) x (16-bit fluorescence intensity for each pixel
736 above baseline) and with all such pixels summed].
737 To determine total volume injected, the maximum fluorescence intensity Sum of
738 all injections within a 2-minute period after injection was determined and used as a
739 proxy for volume injected. To ensure different injections were comparable, the lowest of
740 the Sum values for all injections was used to estimate a 'threshold volume injected'
741 value (26053363 AU). Injections in which this threshold 'volume' was reached within a
742 two-minute period were then analyzed. The flowrate of each injection was calculated by
743 measuring the slope of the injection fluorescence intensity Sum during the injection
744 period (**Figure 1 – figure supplement 2B**). At the same time, GCaMP5 fluorescence
745 intensity ($\Delta F/F$) from the vulval muscle response was quantified. From this, a significant
746 correlation was observed between the slope of the bromophenol blue fluorescence
747 intensity during injection and the vulval muscle GCaMP5 fluorescence peak amplitude
748 (**Figure 1 – figure supplement 2C**). Injections were then binned into two groups
749 depending on the median of all slopes obtained. All calculated slopes lower than the

750 median were categorized as a ‘slow’ injection while injections above the median were
751 categorized as ‘fast’ injections. From this, ‘slow’ injections were seen to elicit lower peak
752 Ca^{2+} amplitudes when compared to ‘fast’ injections (**Figure 1 – figure supplement 2D**).
753 This indicated that the rate at which an injection was performed significantly determined
754 the strength of the resulting vulval muscle Ca^{2+} response but only for injections
755 performed at these lower-than-typical injection pressures (25 psi). Since flowrate did not
756 significantly correlate with Ca^{2+} dynamics at injection pressures greater than 30 psi, to
757 optimize Ca^{2+} responses, and to reduce instances of needles clogging, injection
758 pressures used when testing animal responses were maintained between 30 – 40 psi.

759 **Vulval muscle prodding protocol**

760 To determine if the vulval muscles were receptive to mechanical stimulus, worms were
761 immobilized as per the microinjection protocol. A prodding needle with a 2.7 μm wide tip
762 was positioned next to either the anterior or posterior part of the vulva. To drive a
763 mechanical displacement onto the prodded vulva, a motorized stage was moved at a
764 range of distances (10 – 60 μm) in the direction of the needle to determine the optimum
765 displacement distance. Subsequent experiments used a blunt prodding probe (4.6 μm
766 wide tip), displaced 50 μm for one second. Image sequences were then segmented into
767 paired prodded and unprodded vulval muscle recordings as per the fluorescence
768 recording protocol. Paired Ca^{2+} responses in the 5 s period following the prodding
769 stimulus were averaged and analyzed.

770 **Embryo volume estimation**

771 To estimate the volume of an embryo, brightfield images of injection-induced egg-laying
772 events were collected, and embryos (n = 7) were measured for the lengths of the major

773 (length) and minor (diameter) axes. Measurements were averaged and the diameter
774 was calculated to be 27 μm while average length was 51 μm. Calculated embryo
775 volume was ~30 pL when approximated as a cylinder and ~20 pL when approximated
776 as an ellipsoid. Both measurements were averaged to estimate an approximate average
777 volume per embryo of 25 pL.

778 **Pharmacological assays**

779 Nemadipine: Nemadipine-B (Toronto Research Chemicals Inc.) was dissolved in DMSO
780 to 10 mM and added to melted NGM at 25 μM final concentration prior to media
781 solidification. Control plates containing an equivalent volume of DMSO were made on
782 the same day (0.1% DMSO (v/v) final concentration). Plates were seeded one day prior
783 to the experiment with a 10-fold concentrated OP50 bacteria cultured in B broth. Worms
784 were placed on nemadipine or DMSO plates for at least 1 h prior to microinjections but
785 no longer than 2 h to prevent excess egg accumulation.

786 Floxuridine: Animals were sterilized by exposure to floxuridine as described (Mitchell et
787 al., 1979; Ravi et al., 2018a). In this assay, L4 animals were staged onto NGM plates
788 seeded with OP50, 100 μL of floxuridine (10 mg/mL) was added directly on top of the
789 staged worms and OP50, and animals were incubated at 20 °C for 24 h. Animals were
790 then visually inspected for lack of embryo accumulation prior to selection for
791 microinjection.

792 **Data analyses**

793 Injection-induced Ca^{2+} transients were analyzed for the following characteristics: time to
794 peak, amplitude of peak, time to decay from peak, and whether egg laying occurred. We

795 defined ‘Time to peak’ as the time elapsed between the start of injection onset and
796 when the Ca^{2+} trace had reached its peak GCaMP5/mCherry (ΔR/R) value. ‘Peak
797 amplitude’ was defined as the peak value (ΔR/R). ‘Decay time’ was defined as the time
798 when cytosolic Ca^{2+} levels declined to 37% of their peak value. We chose 37% of the
799 peak value as our cutoff value to allow us to distinguish between different-order kinetics
800 of decay. Individual Ca^{2+} transient peaks were detected using a custom MATLAB script,
801 as described (Ravi et al., 2018b) and then confirmed via visual inspection of the
802 GCaMP5/mCherry traces from fluorescence recordings. Although multiple injections per
803 animal were often performed, quantitative analyses were performed only on the
804 responses elicited by the first injection. Data were omitted from analyses only for cases
805 in which liquid delivery failed (due to a clogged needle or spillage outside of animal).

806 **Statistical analyses**

807 Results were pooled over several days from at least 20 animals (unless otherwise
808 noted). No explicit power analysis was performed prior to the study, but these numbers
809 are in line with prior behavior experiments (Chase et al., 2004; Collins et al., 2016;
810 Collins and Koelle, 2013). Statistical analyses were performed using Prism 8
811 (GraphPad). Isogenic control animals were always tested alongside mutants to account
812 for possible batch effects. Animals were excluded from analyses when liquid delivery
813 failed to spread within the worm (visually determined from brightfield recordings). To
814 determine if there were any statistical differences between the Ca^{2+} responses elicited
815 by injections between wild-type and mutant worms, a Student’s T-Test was performed.
816 In cases in which multiple genotypes or conditions were compared, the data were
817 analyzed by one-way ANOVA. The distributions of responses were tested for normality,

818 and in cases in which data were found to be non-normal, a nonparametric equivalence
819 test was performed (e.g., Mann-Whitney or Kruskal-Wallis). All tests were corrected for
820 multiple comparisons (Bonferroni for ANOVA, Dunn for Kruskal-Wallis). Details of which
821 test was performed for specific strains can be found in figure legends.

822 Standard least squares regression for vulval muscle Ca^{2+} transient amplitude

823 To determine which factor, as a consequence of injection, best predicted the vulval
824 muscle Ca^{2+} response, a standard least squares regression analysis was performed
825 with 'time to peak', 'decay time', 'number of eggs in uterus', and 'flowrate' as factors.
826 From this analysis, only 'number of eggs in uterus' significantly correlated with vulval
827 muscle Ca^{2+} transient amplitude ($p = 0.0095$).

828 Nominal logistic fit for egg laying

829 A similar analysis was performed to determine which factor best predicted egg release
830 following injection. The predictors used were 'vulval muscle Ca^{2+} transient amplitude',
831 'flowrate', 'time to peak', 'decay time', and 'number of eggs in uterus'. Only 'vulval
832 muscle Ca^{2+} transient amplitude was a significant predictor ($p < 0.0001$).

833 **Acknowledgements**
834 We thank Dr. James Baker and members of the Collins Lab for constructive feedback
835 on the manuscript. We thank Dr. Ilya Ruvinsky for helpful discussions. We also thank
836 Drs. Xiaofei Bai and Andy Golden for constructing and providing the AG527 strain and
837 Dr. Addys Bode Hernandez for construction of the MIA136 strain. This work was funded
838 by grants from the National Institutes of Health (NS086932) and the National Science
839 Foundation (IOS-1844657) to KMC. EM was supported by the NSF Graduate Research
840 Fellowship and McKnight Doctoral Fellowship. Some strains were provided by the CGC,
841 which is funded by NIH Office of Research Infrastructure Programs (P40-OD010440).

842 **REFERENCES**

843 Alcaino C, Farrugia G, Beyder A. 2017. Mechanosensitive Piezo Channels in the
844 Gastrointestinal TractCurrent Topics in Membranes. Elsevier. pp. 219–244.
845 doi:10.1016/bs.ctm.2016.11.003
846 Alkema MJ, Hunter-Ensor M, Ringstad N, Horvitz HR. 2005. Tyramine Functions
847 Independently of Octopamine in the Caenorhabditis elegans Nervous System.
848 *Neuron* **46**:247–260. doi:10.1016/j.neuron.2005.02.024
849 Altun ZF, Chen B, Wang Z-W, Hall DH. 2009. High resolution map of *Caenorhabditis*
850 *elegans* gap junction proteins. *Dev Dyn* **238**:1936–1950. doi:10.1002/dvdy.22025
851 Alvarez WC. 1922. THE MYOGENIC NATURE OF THE RHYTHMIC CONTRACTIONS
852 OF THE INTESTINE. *American Journal of Physiology-Legacy Content* **59**:421–
853 430. doi:10.1152/ajplegacy.1922.59.1.421
854 Ann K, Kowalchyk JA, Loyet KM, Martin TFJ. 1997. Novel Ca^{2+} -binding Protein
855 (CAPS) Related to UNC-31 Required for Ca^{2+} -activated Exocytosis. *J Biol*
856 *Chem* **272**:19637–19640. doi:10.1074/jbc.272.32.19637
857 Aprison EZ, Ruvinsky I. 2019. Coordinated Behavioral and Physiological Responses to
858 a Social Signal Are Regulated by a Shared Neuronal Circuit. *Current Biology*
859 S0960982219313181. doi:10.1016/j.cub.2019.10.012
860 Avery L, Thomas JH. 1997. 24 Feeding and Defecation. *Cold Spring Harbor Monograph*
861 *Archive* **33**:679-716–716. doi:10.1101/087969532.33.679
862 Bai X, Bouffard J, Lord A, Brugman K, Sternberg PW, Cram EJ, Golden A. 2020.
863 Caenorhabditis elegans PIEZO channel coordinates multiple reproductive tissues
864 to govern ovulation. *eLife* **9**:e53603. doi:10.7554/eLife.53603
865 Banerjee N, Bhattacharya R, Gorczyca M, Collins KM, Francis MM. 2017. Local
866 neuropeptide signaling modulates serotonergic transmission to shape the
867 temporal organization of C. elegans egg-laying behavior. *PLOS Genetics*
868 **13**:e1006697. doi:10.1371/journal.pgen.1006697
869 Bany IA, Dong M-Q, Koelle MR. 2003. Genetic and Cellular Basis for Acetylcholine
870 Inhibition of *Caenorhabditis elegans* Egg-Laying Behavior. *J Neurosci* **23**:8060–
871 8069. doi:10.1523/JNEUROSCI.23-22-08060.2003
872 Berkowitz LA, Knight AL, Caldwell GA, Caldwell KA. 2008. Generation of Stable
873 Transgenic C. elegans Using Microinjection. *Journal of Visualized Experiments* 3.
874 Brenner S. 1974. The Genetics of Caenorhabditis elegans. *Genetics* **77**:71–94.
875 Brewer JC, Olson AC, Collins KM, Koelle MR. 2019. Serotonin and neuropeptides are
876 both released by the HSN command neuron to initiate Caenorhabditis elegans
877 egg laying. *PLOS Genetics* **15**:e1007896. doi:10.1371/journal.pgen.1007896
878 Chase DL, Koelle MR. 2004. Genetic Analysis of RGS Protein Function in
879 Caenorhabditis elegansMethods in Enzymology. Elsevier. pp. 305–320.
880 doi:10.1016/S0076-6879(04)89018-9
881 Chase DL, Pepper JS, Koelle MR. 2004. Mechanism of extrasynaptic dopamine
882 signaling in Caenorhabditis elegans. *Nat Neurosci* **7**:1096–1103.
883 doi:10.1038/nn1316
884 Collins KM, Bode A, Fernandez RW, Tanis JE, Brewer JC, Creamer MS, Koelle MR.
885 2016. Activity of the C. elegans egg-laying behavior circuit is controlled by

competing activation and feedback inhibition. *eLife* **5**:e21126. doi:10.7554/eLife.21126

Collins KM, Koelle MR. 2013. Postsynaptic ERG potassium channels limit muscle excitability to allow distinct egg-laying behavior states in Caenorhabditis elegans. *J Neurosci* **33**:761–775. doi:10.1523/JNEUROSCI.3896-12.2013

Cook SJ, Jarrell TA, Brittin CA, Wang Y, Bloniarz AE, Yakovlev MA, Nguyen KCQ, Tang LT-H, Bayer EA, Duerr JS, Bülow HE, Hobert O, Hall DH, Emmons SW. 2019. Whole-animal connectomes of both Caenorhabditis elegans sexes. *Nature* **571**:63–71. doi:10.1038/s41586-019-1352-7

Desai C, Horvitz HR. 1989. Caenorhabditis elegans mutants defective in the functioning of the motor neurons responsible for egg laying. *Genetics* **121**:703–721. doi:10.1093/genetics/121.4.703

Dhakal P, Chaudhry SI, Signorelli R, Collins KM. 2022. Serotonin signals through postsynaptic Gαq, Trio RhoGEF, and diacylglycerol to promote *Caenorhabditis elegans* egg-laying circuit activity and behavior. *Genetics* **221**:iyac084. doi:10.1093/genetics/iyac084

Dibb NJ, Brown DM, Karn J, Moerman DG, Bolten SL, Waterston RH. 1985. Sequence Analysis of Mutations that Affect the Synthesis, Assembly and Enzymatic Activity of the uric-54 Myosin Heavy Chain of Caenorhabditis elegans 9.

Farrugia G, Holm AN, Rich A, Sarr MG, Szurszewski JH, Rae JL. 1999. A mechanosensitive calcium channel in human intestinal smooth muscle cells. *Gastroenterology* **117**:900–905. doi:10.1016/S0016-5085(99)70349-5

Fenk LA, de Bono M. 2015. Environmental CO_2 inhibits *Caenorhabditis elegans* egg-laying by modulating olfactory neurons and evokes widespread changes in neural activity. *Proc Natl Acad Sci USA* **112**:E3525–E3534. doi:10.1073/pnas.1423808112

Frøkjær-Jensen C, Kindt KS, Kerr RA, Suzuki H, Melnik-Martinez K, Gerstbreih B, Driscoll M, Schafer WR. 2006. Effects of Voltage-Gated Calcium Channel Subunit Genes on Calcium Influx in Cultured C. elegans Mechanosensory Neurons. *Journal of Neurobiology* **66**. doi:10.1002/neu.20261

Garcia J, Collins KM. 2019. The HSN egg-laying command neurons are required for normal defecation frequency in Caenorhabditis elegans (II). *microPublication Biology*.

Gilpin W, Uppaluri S, Brangwynne CP. 2015. Worms under Pressure: Bulk Mechanical Properties of C. elegans Are Independent of the Cuticle. *Biophysical Journal* **108**:1887–1898. doi:10.1016/j.bpj.2015.03.020

Goodman MB, Sengupta P. 2019. How Caenorhabditis elegans Senses Mechanical Stress, Temperature, and Other Physical Stimuli. *Genetics* **212**:25–51. doi:10.1534/genetics.118.300241

Gou B, Liu Y, Guntur AR, Stern U, Yang C-H. 2014. Mechanosensitive Neurons on the Internal Reproductive Tract Contribute to Egg-Laying-Induced Acetic Acid Attraction in Drosophila. *Cell Reports* **9**:522–530. doi:10.1016/j.celrep.2014.09.033

Guyton AC. 1976. Textbook of Medical Physiology, 5th ed. W. B. Saunders Company.

Hallem EA, Sternberg PW. 2008. Acute carbon dioxide avoidance in Caenorhabditis elegans. *Proceedings of the National Academy of Sciences* **105**:6.

932 Harris JE, Crofton HD. 1957. Structure and Function in the Nematodes: Internal
933 Pressure and Cuticular Structure in Ascaris. *Journal of Experimental Biology*
934 **34**:116–130.
935 Hayes UL, De Vries GJ. 2007. Role of pregnancy and parturition in induction of
936 maternal behavior in prairie voles (Microtus ochrogaster). *Hormones and*
937 *Behavior* **51**:265–272. doi:10.1016/j.yhbeh.2006.10.011
938 Jose AM, Bany IA, Chase DL, Koelle MR. 2007. A Specific Subset of Transient
939 Receptor Potential Vanilloid-Type Channel Subunits in *Caenorhabditis elegans*
940 Endocrine Cells Function as Mixed Heteromers to Promote Neurotransmitter
941 Release. *Genetics* **175**:93–105. doi:10.1534/genetics.106.065516
942 Kandel ER, Schwartz JH, Jessell TM, Siegelbaum SA, Hudspeth AJ. 2012. Principles of
943 Neural Science, 5th ed. New York: McGraw-hill.
944 Kaulich E, Walker DS, Tang Y-Q, Schafer WR. 2021. The Caenorhabditis elegans tmc-
945 1 is involved in egg-laying inhibition in response to harsh touch. *microPublication*
946 *Biology* 6. doi:10.17912/micropub.biology.000439
947 Kendrick KM, Levy F, Keverne EB. 1991. Importance of Vaginocervical Stimulation for
948 the Formation of Matemal Bonding in Primiparous and Multiparous Parturient
949 Ewes. *Physiology & Behavio* **50**:595–600.
950 Kopchock RJ, Ravi B, Bode A, Collins KM. 2021. The Sex-Specific VC Neurons Are
951 Mechanically Activated Motor Neurons That Facilitate Serotonin-Induced Egg
952 Laying in *C. elegans*. *J Neurosci* **41**:3635–3650. doi:10.1523/JNEUROSCI.2150-
953 20.2021
954 Kwok TCY, Ricker N, Fraser R, Chan AW, Burns A, Stanley EF, McCourt P, Cutler SR,
955 Roy PJ. 2006. A small-molecule screen in C. elegans yields a new calcium
956 channel antagonist. *Nature* **441**:91–95. doi:10.1038/nature04657
957 Lagoy R, Kim H, Mello CC, Albrecht DR. 2018. A C. elegans model for the rare human
958 channelopathy, Timothy syndrome type 1. *MicroPubl Biol*
959 10.17912/micropub.biology.000081. doi:10.17912/micropub.biology.000081
960 Lamitina ST, Morrison R, Moeckel GW, Strange K. 2004. Adaptation of the nematode
961 Caenorhabditis elegans to extreme osmotic stress. *American Journal of*
962 *Physiology-Cell Physiology* **286**:C785–C791. doi:10.1152/ajpcell.00381.2003
963 Li P, Collins KM, Koelle MR, Shen K. 2013. LIN-12/Notch signaling instructs
964 postsynaptic muscle arm development by regulating UNC-40/DCC and MADD-2
965 in Caenorhabditis elegans. *eLife* **2**:e00378. doi:10.7554/eLife.00378
966 Lopes G, Bonacchi N, FrazÃ£o J, Neto JP, Atallah BV, Soares S, Moreira L, Matias S,
967 Itskov PM, Correia PA, Medina RE, Calcaterra L, Dreosti E, Paton JJ, Kampff
968 AR. 2015. Bonsai: an event-based framework for processing and controlling data
969 streams. *Front Neuroinform* **9**. doi:10.3389/fninf.2015.00007
970 Lyford GL, Strege PR, Shepard A, Ou Y, Ermilov L, Miller SM, Gibbons SJ, Rae JL,
971 Szurszewski JH, Farrugia G. 2002. α_{1C} (Ca_V 1.2) L-type calcium channel
972 mediates mechanosensitive calcium regulation. *American Journal of Physiology-*
973 *Cell Physiology* **283**:C1001–C1008. doi:10.1152/ajpcell.00140.2002
974 Macosko EZ, Pokala N, Feinberg EH, Chalasani SH, Butcher RA, Clardy J, Bargmann
975 CI. 2009. A hub-and-spoke circuit drives pheromone attraction and social
976 behaviour in C. elegans. *Nature* **458**:1171–1175. doi:10.1038/nature07886

McCarter J, Bartlett B, Dang T, Schedl T. 1999. On the Control of Oocyte Meiotic Maturation and Ovulation inCaenorhabditis elegans. *Developmental Biology* **205**:111–128. doi:10.1006/dbio.1998.9109

Mello CC, Kramer JM, Stinchcomb D, Ambros V. 1991. Efficient gene transfer in C.elegans: extrachromosomal maintenance and integration of transforming sequences. *The EMBO Journal* **10**:3959–3970. doi:10.1002/j.1460-2075.1991.tb04966.x

Mercado-Perez A, Beyder A. 2022. Gut feelings: mechanosensing in the gastrointestinal tract. *Nat Rev Gastroenterol Hepatol* **19**:283–296. doi:10.1038/s41575-021-00561-y

Mitchell DH, Stiles JW, Santelli J, Sanadi DR. 1979. Synchronous Growth and Aging of Caenorhabditis elegans in the Presence of Fluorodeoxyuridine. *Journal of Gerontology* **34**:28–36.

Pan B, Akyuz N, Liu X-P, Asai Y, Nist-Lund C, Kurima K, Derfler BH, György B, Limapichat W, Walujkar S, Wimalasena LN, Sotomayor M, Corey DP, Holt JR. 2018. TMC1 Forms the Pore of Mechanosensory Transduction Channels in Vertebrate Inner Ear Hair Cells. *Neuron* **99**:736-753.e6. doi:10.1016/j.neuron.2018.07.033

Rabinowitch I, Chatzigeorgiou M, Schafer WR. 2013. A Gap Junction Circuit Enhances Processing of Coincident Mechanosensory Inputs. *Current Biology* **23**:963–967. doi:10.1016/j.cub.2013.04.030

Ravi B, Garcia J, Collins KM. 2018a. Homeostatic Feedback Modulates the Development of Two-State Patterned Activity in a Model Serotonin Motor Circuit in Caenorhabditis elegans. *J Neurosci* **38**:6283–6298. doi:10.1523/JNEUROSCI.3658-17.2018

Ravi B, Nassar LM, Kopchock RJ, Dhakal P, Scheetz M, Collins KM. 2018b. Ratiometric Calcium Imaging of Individual Neurons in Behaving Caenorhabditis Elegans. *J Vis Exp*. doi:10.3791/56911

Ravi B, Zhao J, Chaudhry SI, Signorelli R, Bartole M, Kopchock RJ, Guijarro C, Kaplan JM, Kang L, Collins KM. 2021. Presynaptic Gαo (GOA-1) signals to depress command neuron excitability and allow stretch-dependent modulation of egg laying in *Caenorhabditis elegans*. *Genetics* **218**:iyab080. doi:10.1093/genetics/iyab080

Richmond JE, Davis WS, Jorgensen EM. 1999. UNC-13 is required for synaptic vesicle fusion in C. elegans. *Nat Neurosci* **2**:959–964. doi:10.1038/14755

Ringstad N, Horvitz HR. 2008. FMRFamide neuropeptides and acetylcholine synergistically inhibit egg-laying by C. elegans. *Nat Neurosci* **11**:1168–1176. doi:10.1038/nn.2186

Rose AM, Baillie DL. 1980. Genetic Organization of the Region around UNC-15 (I), a Gene Affecting Paramyosin in CAENORHABDITIS ELEGANS. *Genetics* **96**:639–648.

Sawin ER. 1996. Genetic and Cellular Analysis of Modulated Behaviors in Caenorhabditis elegans. *Doctoral dissertation, Massachusetts Institute of Technology*.

Schafer R, Sanchezt BM, Kenyon C. 1996. Genes Affecting Sensitivity to Serotonin in Caenorhabditis elegans. *Genetics* **143**:1219–1230.

1023 Schafer WR. 2006. Genetics of Egg-Laying in Worms. *Annu Rev Genet* **40**:487–509.
1024 doi:10.1146/annurev.genet.40.110405.090527
1025 Schedl T, Kimble J. 1988. fog-2, a germ-line-specific sex determination gene required
1026 for hermaphrodite spermatogenesis in Caenorhabditis elegans. *Genetics*
1027 **119**:43–61. doi:10.1093/genetics/119.1.43
1028 Shao L, Chung P, Wong A, Siwanowicz I, Kent CF, Long X, Heberlein U. 2019. A
1029 Neural Circuit Encoding the Experience of Copulation in Female Drosophila.
1030 *Neuron* **102**:1025-1036.e6. doi:10.1016/j.neuron.2019.04.009
1031 Shyn SI, Kerr R, Schafer WR. 2003. Serotonin and Go Modulate Functional States of
1032 Neurons and Muscles Controlling C. elegans Egg-Laying Behavior. *Current*
1033 *Biology* **13**:1910–1915. doi:10.1016/j.cub.2003.10.025
1034 Suzuki H, Kerr R, Bianchi L, Frøkjær-Jensen C, Slone D, Xue J, Gerstbrein B, Driscoll
1035 M, Schafer WR. 2003. In Vivo Imaging of C. elegans Mechanosensory Neurons
1036 Demonstrates a Specific Role for the MEC-4 Channel in the Process of Gentle
1037 Touch Sensation. *Neuron* **39**:1005–1017. doi:10.1016/j.neuron.2003.08.015
1038 Takahashi K, Hayashi S, Miyajima M, Omori M, Wang J, Kaihara K, Morimatsu M,
1039 Wang C, Chen J, Iribe G, Naruse K, Sokabe M. 2019. L-type calcium channel
1040 modulates mechanosensitivity of the cardiomyocyte cell line H9c2. *Cell Calcium*
1041 **79**:68–74. doi:10.1016/j.ceca.2019.02.008
1042 Taylor SR, Santpere G, Weinreb A, Barrett A, Reilly MB, Xu C, Varol E, Oikonomou P,
1043 Glenwinkel L, McWhirter R, Poff A, Basavaraju M, Rafi I, Yemini E, Cook SJ,
1044 Abrams A, Vidal B, Cros C, Tavazoie S, Sestan N, Hammarlund M, Hobert O,
1045 Miller DM. 2021. Molecular topography of an entire nervous system. *Cell*
1046 **184**:4329-4347.e23. doi:10.1016/j.cell.2021.06.023
1047 Trent C. 1982. Genetic and Behavioral Studies of the Egg-laying System in
1048 Caenorhabditis elegans. *Doctoral Dissertation, Massachusetts Institute of*
1049 *Technology, Cambridge, USA*.
1050 Trent C, Tsung N, Horvitz HR. 1983. EGG-LAYING DEFECTIVE MUTANTS OF THE
1051 NEMATODE *CAENORHABDITIS ELEGANS*. *Genetics* **104**:619–647.
1052 doi:10.1093/genetics/104.4.619
1053 Waggoner LE, Zhou GT, Schafer RW, Schafer WR. 1998. Control of Alternative
1054 Behavioral States by Serotonin in Caenorhabditis elegans. *Neuron* **21**:203–214.
1055 doi:10.1016/S0896-6273(00)80527-9
1056 Walker DS, Schafer WR. 2020. Distinct roles for innexin gap junctions and
1057 hemichannels in mechanosensation. *eLife* **9**:e50597. doi:10.7554/eLife.50597
1058 White JG, Southgate E, Thomson JN, Brenner S. 1986. The Structure of the Nervous
1059 System of the Nematode Caenorhabditis elegans. *Philosophical Transactions of*
1060 *the Royal Society of London Series B, Biological Sciences* **314**:1–340.
1061 Wray S. 1993. Uterine contraction and physiological mechanisms of modulation.
1062 *American Journal of Physiology-Cell Physiology* **264**:C1–C18.
1063 doi:10.1152/ajpcell.1993.264.1.C1
1064 Yue X, Zhao J, Li X, Fan Y, Duan D, Zhang X, Zou W, Sheng Y, Zhang T, Yang Q, Luo
1065 J, Duan S, Xiao R, Kang L. 2018. TMC Proteins Modulate Egg Laying and
1066 Membrane Excitability through a Background Leak Conductance in C. elegans.
1067 *Neuron* **97**:571-585.e5. doi:10.1016/j.neuron.2017.12.041

1068 Zhang M, Chung SH, Fang-Yen C, Craig C, Kerr RA, Suzuki H, Samuel ADT, Mazur E,
1069 Schafer WR. 2008. A Self-Regulating Feed-Forward Circuit Controlling C.
1070 elegans Egg-Laying Behavior. *Current Biology* **18**:1445–1455.
1071 doi:10.1016/j.cub.2008.08.047
1072 Zhang M, Schafer WR, Breitling R. 2010. A circuit model of the temporal pattern
1073 generator of Caenorhabditis egg-laying behavior. *BMC Systems Biology* 9.
1074

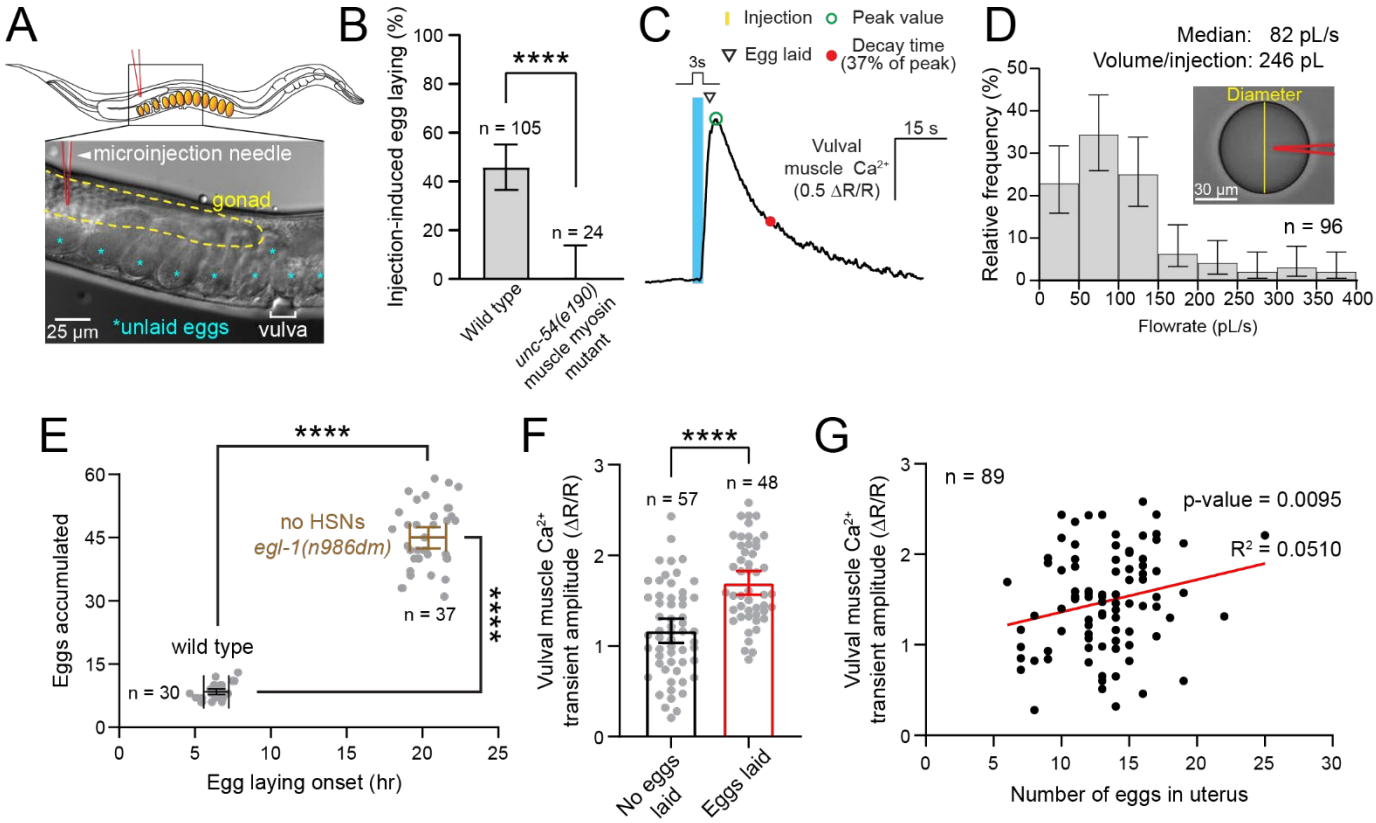

Figure 1: Acute microinjection triggers vulval muscle Ca^{2+} activity and egg-laying behavior.

(A) Cartoon of *C. elegans* and micrograph demonstrating the injection technique. A microinjection needle (arrowhead; red outline) is inserted into the gonad (yellow outline) of an immobilized *C. elegans* worm (top). A 3 s pulse is applied to inject a standard microinjection buffer into the gonad syncytium. Unlaid eggs (cyan asterisks) are then monitored for injection-induced egg release through the vulva (white bracket). **(B)** Bar graphs showing the percent of wild-type or *unc-54(e190)* muscle myosin mutants animals laying eggs in response to injection. Error bars represent ±95% confidence interval for proportions; asterisks indicate p-value < 0.0001 (Fisher's exact test, n indicates number of animals injected per genotype). **(C)** Representative vulval muscle Ca^{2+} trace, determined from GCaMP5/mCherry fluorescence ratio, following a 3 s injection pulse (vertical cyan bar). Key features observed from a typical injection response are egg release (inverted triangle), peak amplitude (ΔR/R; open green circle), and decay time (s; filled red circle; time from peak amplitude to 37%). **(D)** Distribution of estimated injection flowrates obtained by measuring the change in diameter over time of injection buffer drops (yellow vertical line in inserted micrograph) into halocarbon oil immediately following needle withdrawal after worm injection. Error bars represent ±95% confidence interval for the mean proportion across 96 injections. **(E)** Scatterplot of time to egg-laying onset and number of eggs accumulated at egg-laying onset in wild-type (black) and *egl-1(n986dm)* HSN-deficient mutant animals (brown). Asterisks indicate p-value < 0.0001 (unpaired t-tests for differences in egg-laying onset and in egg accumulation). **(F)** Bar graphs comparing mean vulval muscle Ca^{2+} transient amplitudes

1099 (±95% confidence interval) after injections that did not (black) and those that did (red)
1100 result in egg release. Points in scatterplot show responses in individual animals.
1101 Asterisks indicate p-value < 0.0001 (unpaired t-test). **(G)** Scatter plot, with a bivariate
1102 linear regression comparing the relationship between the number of eggs accumulated
1103 inside the uterus at the time of injection and the peak vulval muscle Ca^{2+} response
1104 following injection (p-value = 0.0095; standard least squares regression for vulval
1105 muscle Ca^{2+} transient amplitude; see 'statistical analyses' in methods).

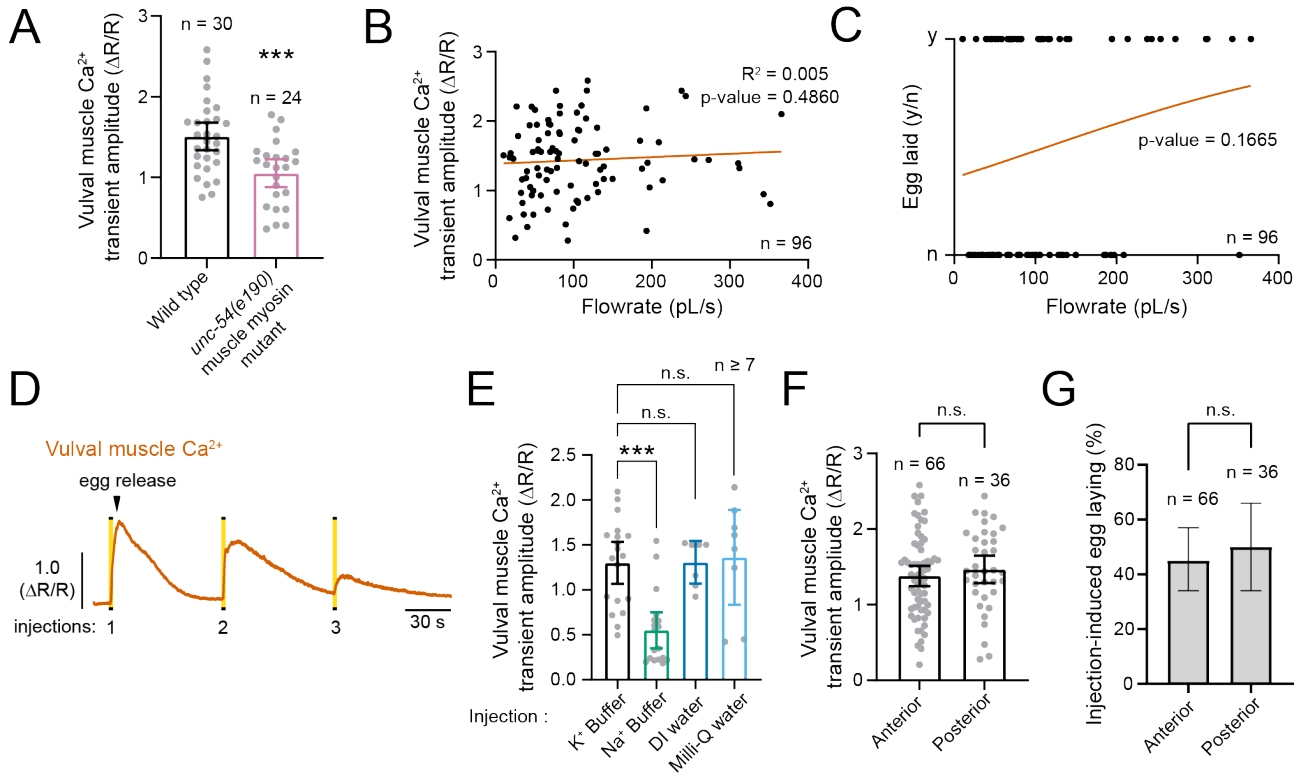

Figure 1 – figure supplement 1: Optimization of the injection protocol. **(A)** Bar graphs comparing the mean injection-induced vulval muscle Ca^{2+} transient amplitudes following injection into wild-type or *unc-54(e190)* muscle myosin mutant animals (± 95% confidence intervals). Points in scatterplot show responses in individual animals. Asterisks indicate p-value = 0.0004 (unpaired t-test). **(B)** Scatterplot with linear regression (red line) of relationship between injection flowrate and resulting vulval muscle Ca^{2+} transient amplitude; p-value = 0.4860 (not significant; standard least squares regression for vulval muscle Ca^{2+} transient amplitude; see 'statistical analyses' in methods). **(C)** Logistic regression comparing the relationship between injection flowrate and egg release. Binomial responses with successful egg release (y) and no egg release (n); p-value = 0.1665 (nominal logistic fit for egg laid; see 'statistical analyses' in methods). **(D)** Representative Ca^{2+} trace after sequential injections into a single animal. Vertical yellow lines represent injection pulses and orange trace indicates resulting vulval muscle Ca^{2+} activity. A single egg-laying event following the first injection is indicated with an inverted triangle. **(E)** Bar graph with scatterplot showing mean vulval muscle Ca^{2+} transient amplitude (±95% confidence intervals) after a 3 s injection with K^+ buffer (black, n = 19), Na^+ buffer (green, n = 18), deionized water (blue, n = 7), or Milli-Q water (cyan, n = 8). Asterisks indicate p-value = 0.003; n.s. indicates p-value > 0.05 (Kruskal-Wallis test with Dunn's correction for multiple comparisons). Average bar graphs with scatterplot showing vulval muscle Ca^{2+} transient amplitude **(F)** or percent of injection-induced egg laying **(G)** when injections were performed into either anterior or posterior gonad.

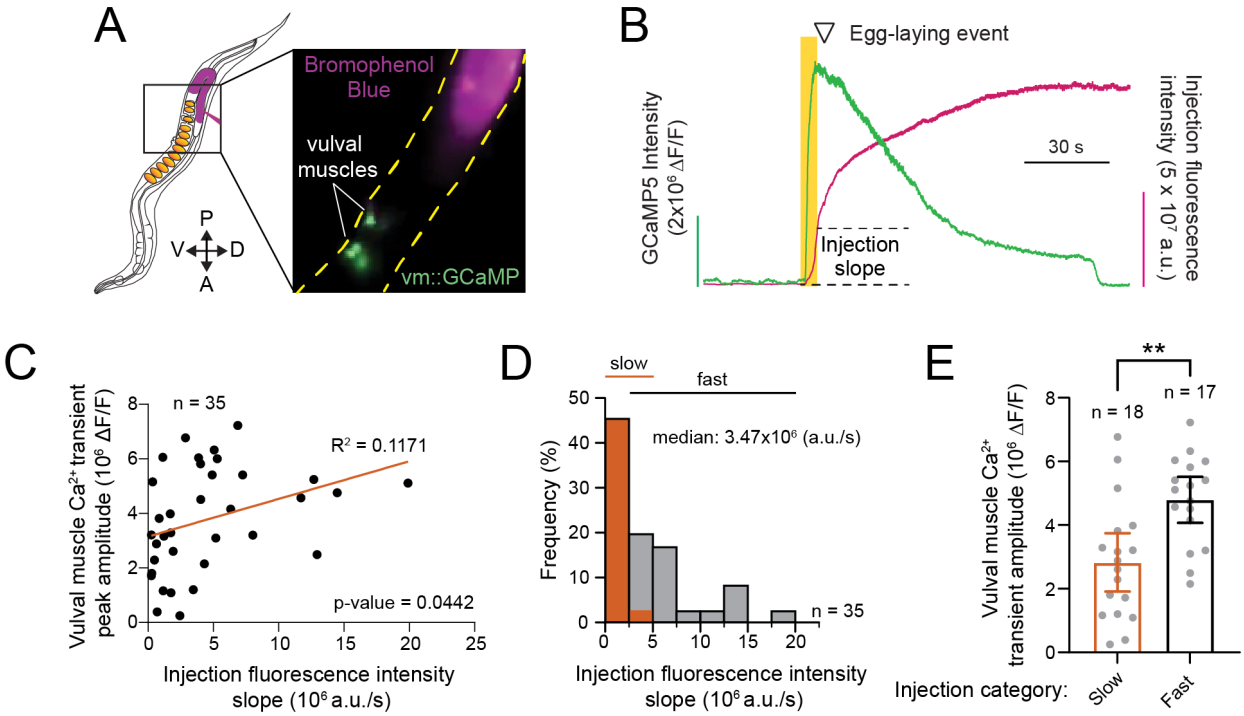

Figure 1 – figure supplement 2: Quantifying correlation of injection flowrate and vulval muscle Ca^{2+} responses using bromophenol blue.
(A) Cartoon of *C. elegans* and micrograph demonstrating injection with bromophenol blue reporter (magenta). Dashed yellow lines represent ventral and dorsal border of animal injected with bromophenol blue (magenta) and the resulted GCaMP5 (green) fluorescence in the vulval muscles (vm). **(B)** Representative traces of vulval muscle GCaMP5 (green; left axis) and bromophenol blue fluorescence (magenta; right axis) after injection used to estimate flowrate and volume delivered. Yellow vertical bar represents time of injection and dotted line represents the change in bromophenol blue fluorescence used to estimate volume injected per 3 s injection time (slope). **(C)** Scatterplot showing significant correlation between injection fluorescence intensity slope and the resulting vulval muscle Ca^{2+} transient peak amplitude across 35 injected animals (p-value = 0.0442). **(D)** Distribution of all injection fluorescence intensity slopes obtained. Slopes were binned as 'slow' (highlighted in orange) or 'fast' depending on whether they were below or above the median slope, respectively. **(E)** Bar graphs with scatterplot showing the mean vulval muscle Ca^{2+} transient peak amplitudes seen with 'slow' or 'fast' injections binned based on slope. Asterisks indicate p-value = 0.0012 (unpaired t-test, n ≥ 17 per group).

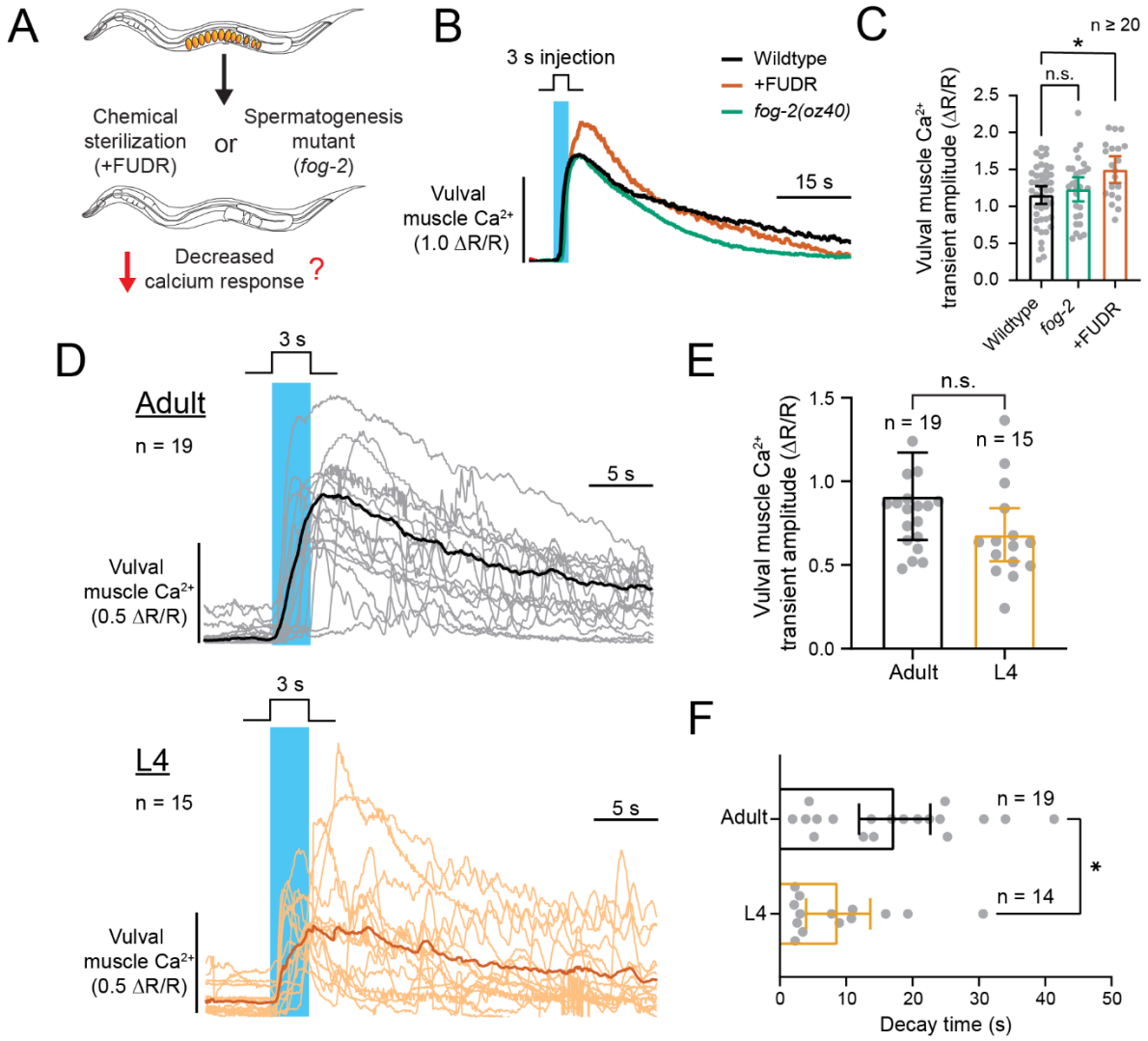

Figure 2: Vulval muscle injection response is independent of egg availability or reproductive maturation.

(A) Diagram of experimental rationale. Floxuridine (FUDR)-treated wild-type or *fog-2(oz40)* sperm-deficient mutant animals were injected and vulval muscle Ca^{2+} activity was followed using GCaMP5. Orange ovals represent fertilized embryos in the uterus of control animals. **(B)** Representative injection-induced vulval muscle Ca^{2+} responses of control wild-type (black), wild-type sterilized with FUDR (red), and *fog-2(oz40)* mutant animals (green). **(C)** Bar graphs with scatterplot showing mean vulval muscle Ca^{2+} transient amplitudes following microinjection. Asterisk indicates p-value = 0.0105, and n.s. indicates p-value > 0.05 (Kruskal-Wallis with Dunn's correction for multiple comparisons; n ≥ 20 animals per condition). **(D)** Injection-induced Ca^{2+} responses for 1-day old adult (top; black trace) and late-L4 (bottom; orange trace) animals. Solid lines show the average Ca^{2+} responses, and lighter lines show responses from individual animals (adults, n = 19; L4 juveniles, n = 15). **(E-F)** Bar graphs with scatterplots showing mean vulval muscle Ca^{2+} amplitudes **(E)** and decay times **(F)**. Asterisk

1164 indicates p-value = 0.0139; n.s. indicates p-value > 0.05 (Mann-Whitney test). Vertical
1165 cyan bars show timing of 3 s microinjection. To facilitate comparisons, one data point
1166 with vulval muscle Ca^{2+} transient amplitude value of 2.99 (ΔR/R) from an adult animal is
1167 not visible in D and E.

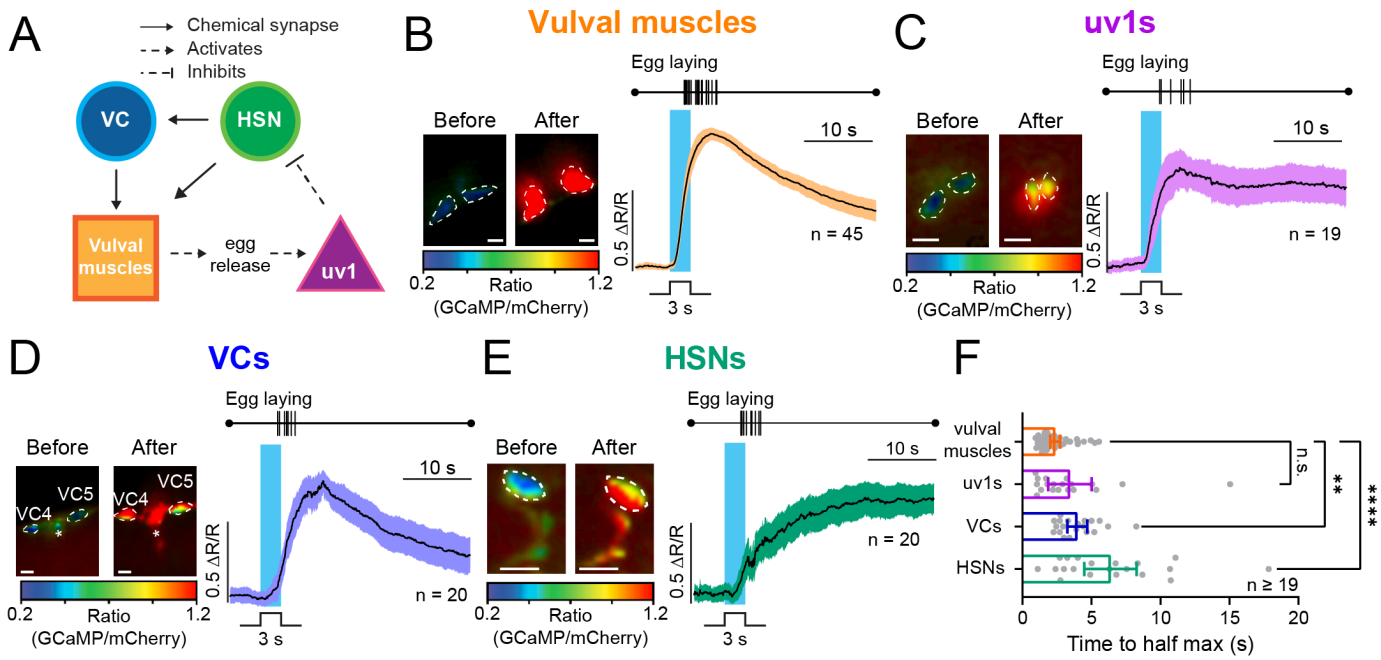

Figure 3: Acute microinjection induces sequential Ca^{2+} activity across the entire egg-laying behavior circuit.
(A) Connectivity of the *C. elegans* egg-laying circuit (adapted from Collins et al., 2016). **(B-E)** Egg laying and normalized Ca^{2+} responses of the vulval muscles **(B)**, uv1 neuroendocrine cells **(C)**, VC motoneurons (**D**), and HSN command motoneurons **(E)**, before and after a 3 s microinjection. Vertical lines show timing of egg-laying events pooled from all injected animals. Micrographs show Ca^{2+} activity in cell bodies (outlined in white) before and after injection; rainbow scale indicates GCaMP5/mCherry ratio in responding cells; blue indicates low Ca^{2+} and red indicates elevated Ca^{2+}. White scale bar indicates 10 µm. Black solid line is a trace of the average Ca^{2+} response; colored bands indicate the 95% confidence interval (n ≥ 19 animals per trace). Vertical cyan line shows 3 s injection period. **(F)** Bar graphs with scatter plots showing time of half-max Ca^{2+} responses. **** indicates p-value < 0.0001, ** indicates p-value = 0.0013, and n.s. indicates p-value > 0.05 (Kruskal-Wallis test with Dunn's correction for multiple comparisons).

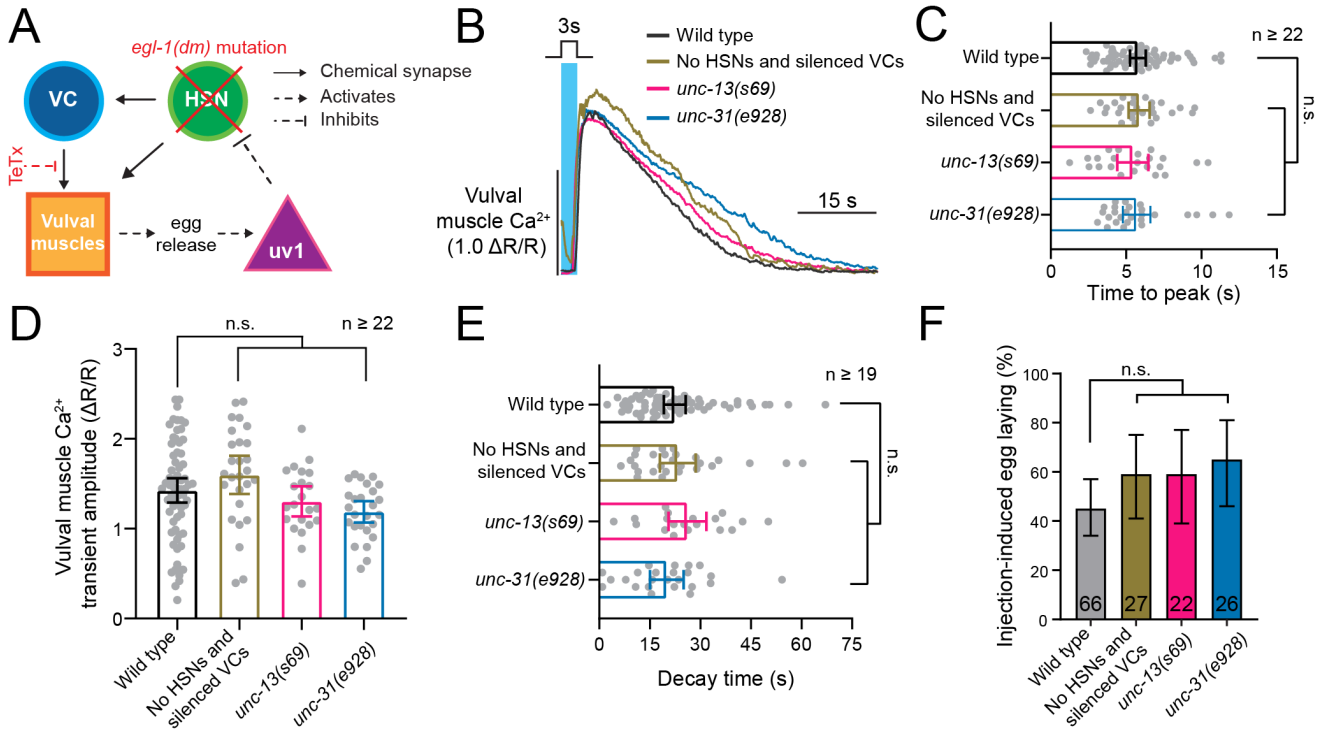

Figure 4: The vulval muscle Ca^{2+} and egg-laying response to microinjection does not require synaptic or peptidergic input.
(A) Diagram highlighting the synaptic connections between cells of the *C. elegans* egg-laying circuit. Red "x" symbol on top of the HSNs represents the genetic removal of any input from the HSNs cells through use of *egl-1(n986dm)* mutants which lack HSN neurons. Tetanus Toxin (TeTx) was also transgenically expressed in the VC neurons to block neurotransmitter release. **(B)** Representative injection-induced vulval muscle Ca^{2+} responses of wild-type (black), HSN-deficient *egl-1(dm)* mutants co-expressing Tetanus Toxin in the VCs (brown), *unc-13(s69)* mutants with defective synaptic transmission, (magenta), and *unc-31(e928)* mutant animals with defective peptidergic transmission (blue). Vertical cyan bar represents the 3 s gonad injection. **(C-E)** Bar graphs with scatter plot showing mean time to vulval muscle Ca^{2+} transient peak (**C**), Ca^{2+} transient peak amplitude (**D**), and Ca^{2+} transient decay times (**E**) following injections (error bars represent mean ±95% confidence intervals). n.s. indicates p-value > 0.05 (one-way ANOVA with Bonferroni's correction for multiple comparisons). **(F)** Bar graphs showing percent of injections that resulted in an egg-laying event (mean ±95% confidence intervals for the proportion); n.s. indicates p-value > 0.05 (Fisher's exact test with Bonferroni's correction for multiple comparisons). Numbers inside bar graph indicate sample sizes; n ≥ 19 animals for all conditions.

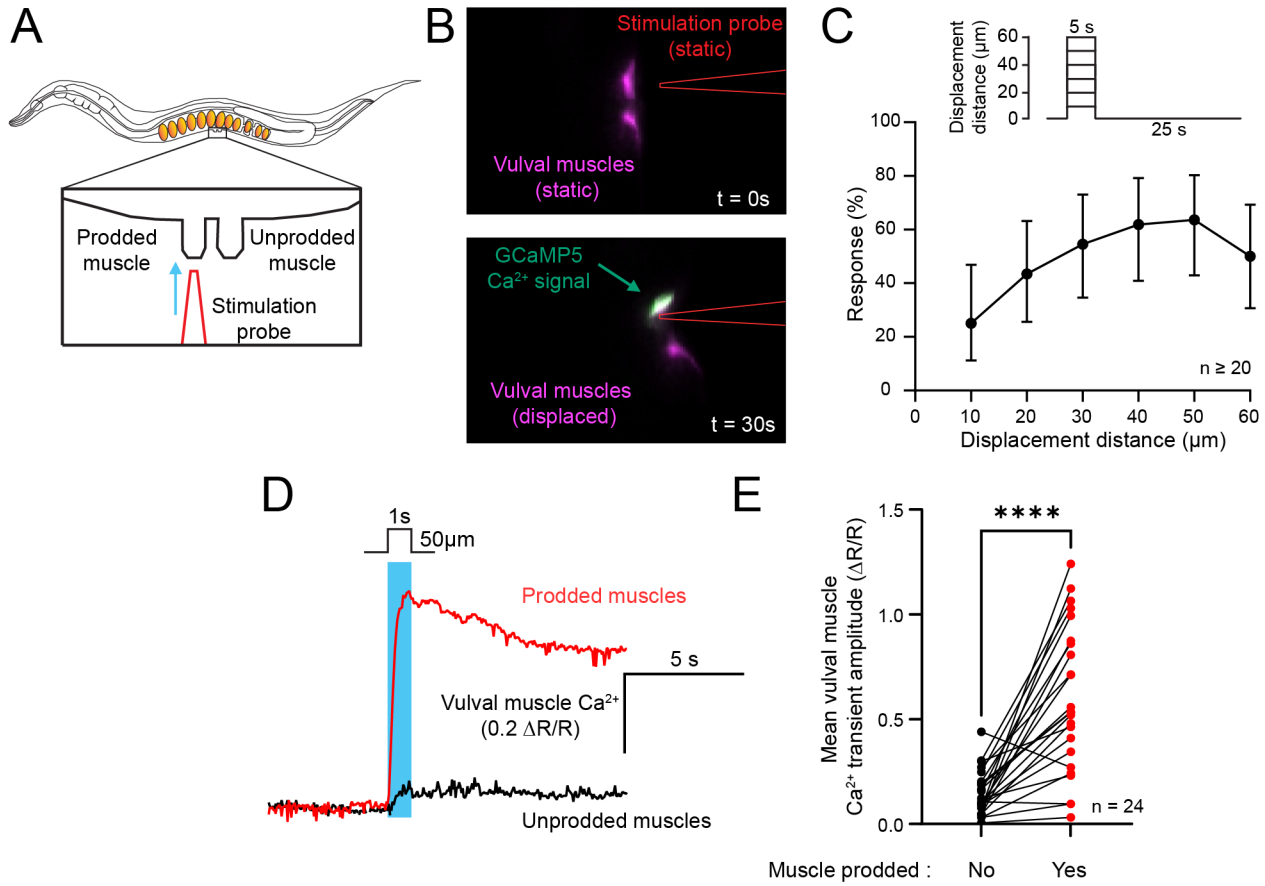

Figure 5: The vulval muscles are receptive to direct mechanical input. **(A)** Diagram of experimental rationale. A glass capillary probe was used to mechanically stimulate either the anterior or posterior vulval muscles while observing changes in vulval muscle Ca^{2+} activity. **(B)** Representative still images of vulval muscle mCherry (magenta) and GCaMP5 (green) fluorescence prior to (top, t = 0 s) or immediately after (bottom, t = 30 s) mechanical stimulation with a stimulation probe (red outline). **(C)** Prodding protocol (top) in which the vulval muscles were prodded for 5 s every 30 s with increasing displacement distances (10 µm steps). Dose-response curve (bottom) showing the relationship between the displacement distance placed upon the vulval muscles and the percent of prodding events that resulted in a vulval muscle Ca^{2+} response (error bars represent ±95% confidence interval for proportions). **(D)** Representative vulval muscle Ca^{2+} traces following a 1 s prodding pulse (vertical cyan line) in unprodded (black, bottom trace) and prodded (red, top trace) vulval muscles. **(E)** Pair-wise comparison of the mean vulval muscle Ca^{2+} responses 5 s in the unprodded (black dots) and their adjacent prodded muscles (red dots). Asterisks indicate p-value < 0.0001 (paired t-test, n > 20 animals).

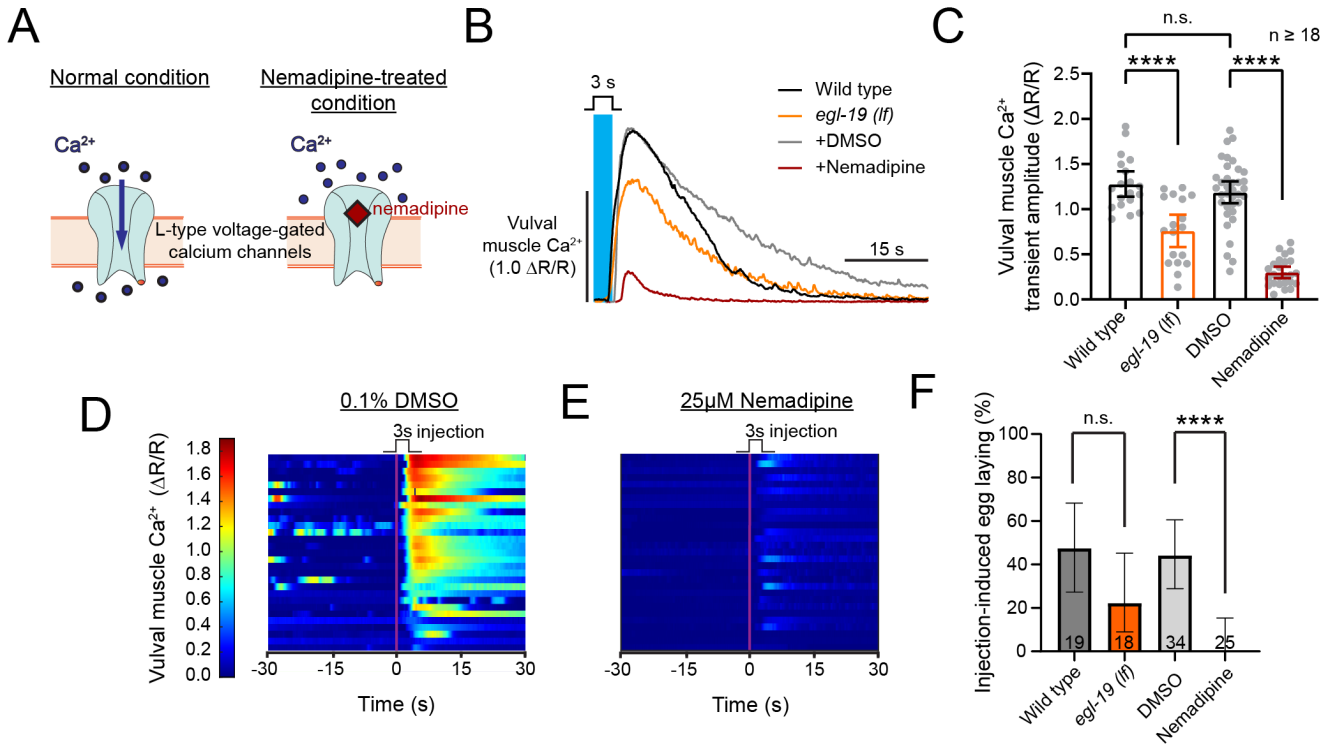

Figure 6: L-type voltage-gated Ca^{2+} channels are required for the vulval muscle injection response.
(A) Diagram (adapted from Lagoy et al., 2018) of experimental treatments. Worms were placed on NGM plates containing either DMSO (normal condition) or 25 μM nemadipine. **(B)** Representative injection-induced vulval muscle Ca^{2+} responses for wild-type (black) or *egl-19(n582)* voltage-gated Ca^{2+} channel loss-of-function mutant animals (orange), worms exposed to 0.1% DMSO (grey), and worms exposed to 25 μM nemadipine (burgundy). Vertical cyan bar represents 3 s injection pulse. **(C)** Bar graphs with scatterplot of mean vulval muscle Ca^{2+} transient amplitude in wild-type (black), *egl-19(lf)* (orange), 0.1% DMSO-treated worms (grey), and nemadipine-treated animals (burgundy) after injection. Asterisks indicates p-value < 0.0001 and n.s. indicates p-value > 0.05 (one-way ANOVA with Bonferroni's correction for multiple comparisons; n ≥ 18 animals). **(D-E)** Heatmaps of vulval muscle Ca^{2+} before and after injections in animals treated for ~2 hours with either 0.1% DMSO **(D)** or 25 μM nemadipine **(E)**. Each row represents Ca^{2+} responses from an individual animal (n>20 animals). Negative time values represent vulval muscle Ca^{2+} activity prior to the injection, vertical purple line represents the start of the 3 s injection, and the diagram above the heatmap indicates the 3 s injection pulse. **(F)** Bar graphs showing percent of injections that resulted in an egg-laying event (mean ±95% confidence intervals for the proportion). Numbers inside bar graph indicate sample sizes; n ≥ 18 animals per condition. Asterisks indicate p-value < 0.0001; n.s. p-value > 0.05 (Pairwise Fisher's exact test).

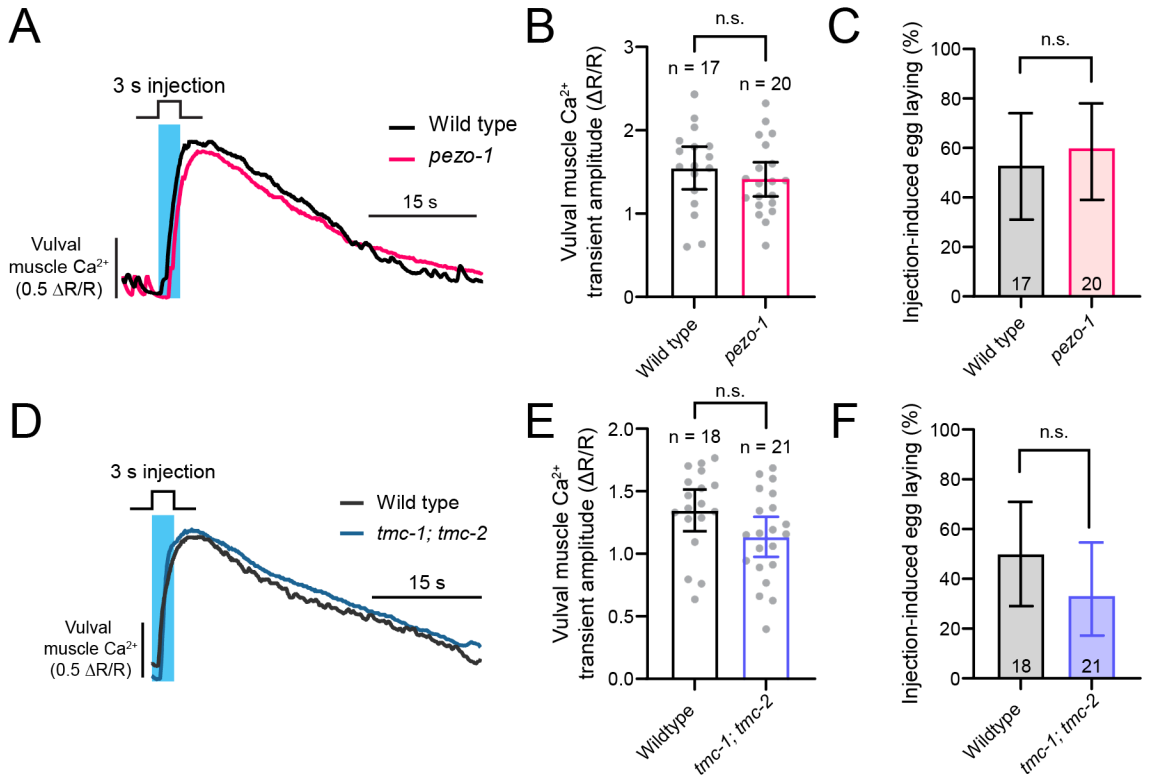

Figure 7: PIEZO and TMC channels are not required for the injection-induced vulval muscle Ca^{2+} and egg-laying response.

(A) Representative injection-induced vulval muscle Ca^{2+} traces after injection into wild-type (black) and *pezo-1(av149)* mutant animals (magenta). **(B)** Bar graphs with scatterplot showing mean vulval muscle Ca^{2+} responses of wild-type (black, n = 17) and *pezo-1* mutants (magenta, n = 20). Error bars indicate 95% confidence interval; n.s. indicates p-value > 0.05 (unpaired t-test). **(C)** Bar graphs showing percent of injections that resulted in an egg-laying event (mean ±95% confidence intervals for the proportion); n.s. indicates p-value > 0.05 (Fisher's exact test) **(D)** Representative injection-induced vulval muscle Ca^{2+} traces after injection into wild-type (black) and *tmc-1(ok1859); tmc-2(ok1302)* double mutant animals (blue). **(E)** Bar graphs with scatterplot showing mean vulval muscle Ca^{2+} responses of wild-type (black, n = 18) and *tmc-1; tmc-2* double mutants (blue, n = 21). Error bars indicate 95% confidence interval for the mean; n.s. indicates p-value > 0.05 (unpaired t-test). **(F)** Bar graphs showing percent of injections that resulted in an egg-laying event (mean ±95% confidence intervals for the proportion); n.s. indicates p-value > 0.05 (Fisher's exact test). Vertical cyan bars indicate 3 s injection. Numbers inside bar graphs indicate sample sizes.

1262 **Table 1: List of *C. elegans* strains used in this study**

STRAIN	GENOTYPE	FEATURE	FIGURE(S)	REFERENCE
N2	Wild type	Bristol wild type	1	(Brenner, 1974)
CB190	*unc-54(e190) I*	Myosin heavy chain null mutant	1	(Brenner, 1974)
LX1918	*vsIs164 lite-1(ce314) lin-15(n765ts) X*	Vulval muscles expressing GCaMP5, mCherry	1 – 6, Figure 1 – supplement 2	(Collins et al., 2016)
MIA206	*unc-54(e190) I; vsIs164 lite-1(ce314) lin-15(n765ts) X*	Myosin heavy chain null mutant with GCaMP5 and mCherry reporters expressed in vulval muscles	Figure 1 – supplement 1, 1	This study
MIA26	*egl-1(n986dm) V*	No HSNs	1	(Garcia and Collins, 2019)
MIA289	*keyIs33; egl-1(n986dm) V; vsIs164 lite-1(ce314) lin-15(n765ts) X*	Lacks HSN neurons, expresses Tetanus Toxin in the VC neurons, and expresses GCaMP5/mCherry in vulval muscles	4	This study
MIA312	*unc-31(e928) IV; vsIs164 lite-1(ce314) lin-15(n765ts) X*	Dense core vesicle release mutant deficient in neuropeptide signaling. Also expresses GCaMP5 and mCherry in vulval muscles	4	This study
MIA316	*unc-13(s69) I; vsIs164 lite-1(ce314) lin-15(n765ts) X*	Synaptic vesicle fusion mutant deficient in neurotransmitter signaling. Also expresses GCaMP and mCherry in vulval muscles	4	This study
MIA136	*lite-1(ce314) lin-15(n765ts) keyIs34 X*	Expresses GCaMP5 and mCherry in uv1 neuroendocrine cells	3	This study
LX1960	*vsIs172; lite-1(ce314) lin-15(n765ts) X*	Expresses GCaMP and mCherry in VC neurons	3	(Collins et al., 2016)
LX2004	*lite-1(ce314) lin-15(n765ts) vsIs183 X*	Expresses GCaMP and mCherry in HSN neurons	3	(Collins et al., 2016)

MIA34	*fog-2(oz40) V; lite-1(ce314) lin-15(n765) vsIs164 X*	Spermatogenesis mutants	2	(Schedl and Kimble, 1988)
MIA51	*keyIs12; lite-1(ce314) lin-15(n765ts) X*	Expresses GCaMP5 and mCherry in vulval muscles from the *ceh-24* promoter for better expression in L4 animals.	2	(Ravi et al., 2018b)
MIA185	*egl-19(n582) IV; lite-1(ce314) lin-15(n765ts) vsIs164 X*	L-type voltage-gated calcium channel loss of function mutant with vulval muscle GCaMP5 and mCherry	6	(Trent et al., 1983)
AG527	*pezo-1 (av149); lite-1(ce314) lin-15(n765ts) vsIs164 X*	*pezo-1* mechanosensory channel mutant with vulval muscle GCaMP5 and mCherry	7	This study
MIA485	*vsIs165*	Integrated transgenic mutant expressing vulval muscle GCaMP5 and mCherry without *lite-1* mutation normally used to prevent blue light avoidance	7	This study
MIA486	*tmc-1(ok1859) X; vsIs165*	Transmembrane channel-like protein mutant with vulval muscle GCaMP5/mCherry	7	This study
MIA487	*tmc-2(ok1302) X; vsIs165*	Transmembrane channel-like protein mutant with vulval muscle GCaMP5/mCherry	7	This study
MIA494	*tmc-1(ok1859), tmc-2(ok1302) X; vsIs165*	Double mutant for *tmc-1* and *tmc-2* with vulval muscle GCaMP5/mCherry	7	This study

1263

1264 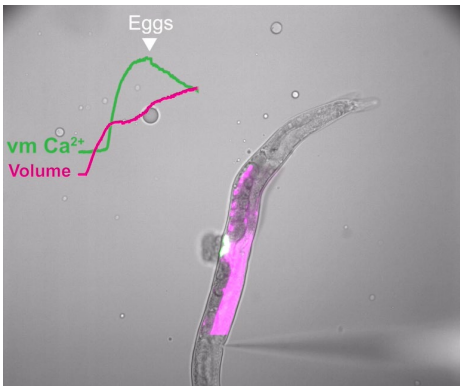

1265 **Movie 1**

1266 Recording of vulval muscle GCaMP5 (green) and bromophenol blue (magenta)
1267 fluorescence during microinjection overlayed over a brightfield recording of *C. elegans.*
1268 Wild-type animals display an increase in vulval muscle (vm) Ca^{2+} activity that correlates
1269 with the increase in injection volume (represented as traces within the video). Egg
1270 release is coincident with peak vulval muscle GCaMP5 fluorescence.

1271 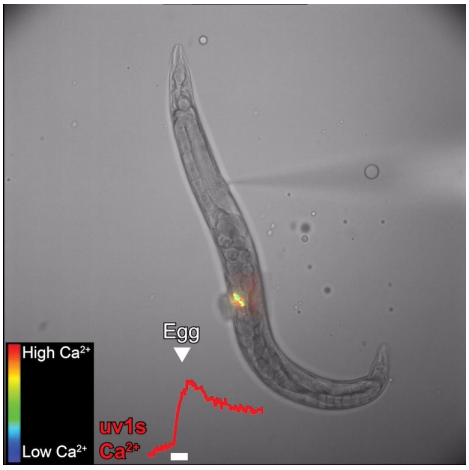

1272 **Movie 2**

1273 GCaMP5 to mCherry fluorescence ratio in uv1 cells of wild-type animals overlaid on top
1274 of brightfield recording during injection. Blue indicates low Ca^{2+}, and red indicates high

1275 Ca^{2+}. Red trace denotes uv1 Ca^{2+} response, triangle denotes egg release, and white

1276 horizontal bar denotes timing of the 3 s injection pulse.

1277 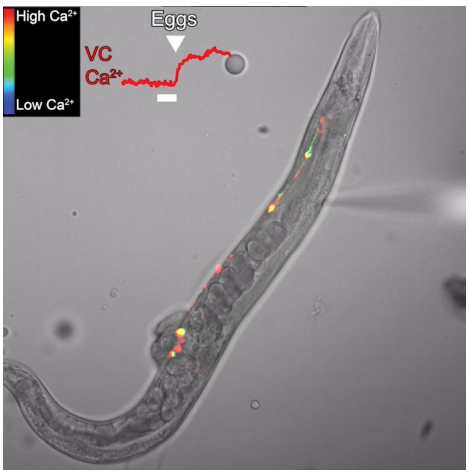

1278 **Movie 3**

1279 GCaMP5 to mCherry fluorescence ratio in VC neurons of wild-type animals overlaid on

1280 top of brightfield recording during injection. Blue indicates low Ca^{2+}, and red indicates

1281 high Ca^{2+}. Red trace denotes VC Ca^{2+} response, triangle denotes egg release, and

1282 white horizontal bar denotes timing of the 3 s injection pulse.

1283 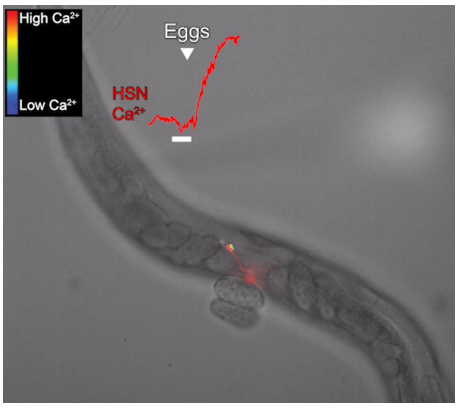

1284 **Movie 4**

1285 GCaMP5 to mCherry fluorescence ratio in HSN neurons of wild-type animals overlaid

1286 on top of brightfield recording during injection. Blue indicates low Ca^{2+}, and red

1287 indicates high Ca^{2+}. Red trace denotes HSN Ca^{2+} response, triangle denotes egg

1288 release, and white horizontal bar denotes timing of the 3 s injection pulse.

1289 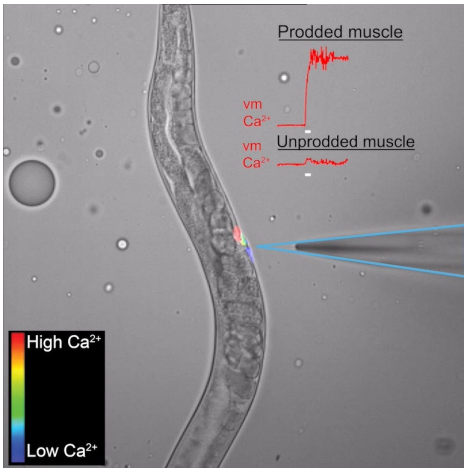

1290 **Movie 5**

1291 Recording of vulval muscle mCherry (magenta) and vulval muscle GCaMP5 (green)

1292 fluorescence during mechanical prodding of the posterior but not anterior vulval

1293 muscles. Cyan outline border of the prodding needle. White horizontal bar denotes

1294 timing of 1 s prodding stimulus.

1295 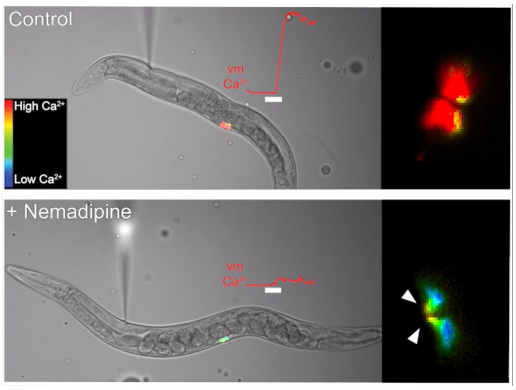

1296 **Movie 6**

1297 GCaMP5 to mCherry fluorescence ratio in vulval muscles of a DMSO-treated control

1298 animal (top) and a nemadipine-treated animal (bottom) overlaid on top of respective

1299 brightfield recording during injection. Blue indicates low Ca^{2+}, and red indicates high
1300 Ca^{2+}. Red traces denote vulval muscle Ca^{2+} responses and white horizontal bar denotes
1301 timing of the 3 s injection pulse. Inserts on right side of movie show a zoomed in
1302 recording of vulval muscle Ca^{2+} response for control and Nemadipine-treated animals to
1303 emphasize localization of Ca^{2+} activity. White arrowhead shows localization of residual
1304 Ca^{2+} activity from vm1 muscles in nemadipine-treated animals.